Male-preferred glycolysis and female-preferred fatty acid utilization for ATP production in skeletal muscles bestowed by Pfkfb3 and Pdk4

アントニアス, クリスティアント

Male-preferred glycolysis and female-preferred fatty acid utilization for ATP production in skeletal muscles bestowed by *Pfkfb3* and *Pdk4*

Antonius Christianto

Laboratory of Biology of Sex Differences

Division of Medical Molecular Cell Biology

Graduate School of Systems Life Sciences

Kyushu University

2021

List of abbreviation

Actb	β-actin
Amd	S-adenosylmethionine decarboxylase
AR	androgen receptor
BSA	bovine serum albumin
Cas	castration
Col	collagen
COXIV	cytochrome c oxidase subunit 4
CPM	counts per million mapped reads
Cpt1b	carnitine palmitoyltransferase 1B
CSA	cross sectional area
CTR	control
DAPI	4’,6’-diamidino-2-phenylindole
DHT	dihydrotestosterone
DMEM	dulbecco’s modified eagle medium
E2	estradiol
ECAR	extracellular acidification rate
ECM	extracellular matrix
EDTA	ethylenediaminetetraacetic acid
EGTA	egtazic acid
ER	estrogen receptor
F-2,6-BP	fructose-2,6-bisphosphate
F-6-P	fructose-6-phosphate
FBS	fetal bovine serum
Gapdh	glyceraldehyde 3-phosphate dehydrogenase

GO	gene ontology
Hadhb	hydroxyacyl-CoA dehydrogenase
HIF1α	hypoxia inducible factor 1α
HRT	hormone replacement treatment
IMCT	intracellular connective tissue
KD	knockdown
M-MLV	moloney murine leukemia virus
MAS	matsunami adhesive silane
MYH	myosin heavy chain
MYH1	myosin heavy chain type I
MYH2	myosin heavy chain type II
MYH2A	myosin heavy chain type IIA
MYH2B	myosin heavy chain type IIB
MYH4	myosin heavy chain type IV
MYH7	myosin heavy chain type VII
NADPH	nicotinamide adenine dinucleotide phosphate
NR3C4	nuclear receptor subfamily 3, group C, gene 4
OCR	oxygen consumption rate
Odc1	ornithine decarboxylase 1
Ovx	ovariectomy
P-PDH	phosphorylated-pyruvate dehydrogenase
PBS	phosphate-buffered saline
PCA	principal component analysis
Pcx	pyruvate carboxylase
PDH	pyruvate dehydrogenase
Pdk4	pyruvate dehydrogenase kinase 4

Pfkfb3	phosphofructokinase-2/6-Phosphofructo-2-Kinase/Fructose-2,6-Biphosphatase 3
PFKM	the type of phosphofructokinase-1 found in muscles
PS	penicillin-streptomycin
qRT-PCR	quantitative RT-PCR
RIPA	radioimmunoprecipitation assay
SD	standard deviation
SDS	sodium dodecyl sulfate
siRNA	small interfering RNA
Smox	spermine oxidase
TBS-T	tris-buffered saline containing 0.1% tween 20

Table of Contents

LIST OF TABLES

ABSTRACT

Skeletal muscles are comprised of several types of fibers characterized in part by their preferential energy production. Skeletal muscles exhibit sexually dimorphic features. As for the biochemical features, glycolysis and fatty acid β-oxidation are predominately active in the muscles of males and females, respectively. However, the mechanisms underlying of the preferential utilization of these fuels remains elusive. The aim of this study is to investigate the possible mechanism causing the sexual dimorphism in the energy metabolism of muscle fiber type IIB.

Mice were gonadectomized and thereafter treated with sex steroids. Type IIB fibers of quadriceps muscles were used for transcriptome analysis. Eventually, I obtained transcriptomes from the fibers of untreated, gonadectomized, and sex steroid-treated mice of both sexes. 68 and 60 genes were obtained as male-enriched and female-enriched genes, respectively. Gene ontology analyses revealed that the male-enriched genes are related to broad range of metabolic processes, while the female-enriched genes are related to extracellular matrix.

Furthermore, analyses of the transcriptomes resulted in finding of two genes, *Pfkfb3* (*phosphofructokinase-2*) and *Pdk4* (*pyruvate dehydrogenase kinase 4*), that may function as switches between the sexually dimorphic metabolic pathways, male-preferred glycolysis and female-preferred fatty acid β-oxidation. Interestingly, *Pfkfb3* and *Pdk4* exhibit male-enriched and estradiol-enhanced expression, respectively.

Additionally, the contribution of these genes to sexually dimorphic metabolism is demonstrated by knockdown studies with cultured type IIB muscle fibers. Taking into consideration that skeletal muscles as a whole are the largest energy-consuming organs, our results provide insights into energy metabolism in the two sexes, during the estrus cycle in women/female, and under pathological conditions involving skeletal muscles.

INTRODUCTION

A wide variety of sex differences have developed in animal structures and functions. Most often, this sexual dimorphism is most obvious in the reproductive system. However, many animals also exhibit sexually dimorphic appearances involving body size, exterior body parts, and feather color. Even many mammalian species display visually appealing features that differ between males and females. Skeletal muscle represents an organ whose structures and activities differ between the two sexes (Haizlip *et al.*, 2015).

Skeletal muscles are one of the three muscle tissues in mammalian bodies. They attached to bones by tendons. The combined structure of muscles and tendons produces forces to move. This primary action of the skeletal muscle is executed through its intrinsic excitation-contraction coupling process. The contraction of the muscle leads to movement of the attached bone. Thousands of muscle fibers are wrapped together by connective tissue sheaths to form a skeletal muscle. Each muscle is made up of groups of muscle fibers called fascicles (Frontera & Ochala, 2015).

A skeletal muscle is composed of different types of fibers that differ in terms of their morphological, biochemical, and physiological properties. According to the expression of the myosin heavy chain (MYH) gene in rodents, these fibers are largely divided into four types (types I, IIA, IIB, and IIX) (Schiaffino *et al.*, 1989; Pette & Staront, 1997; Schiaffino & Reggiani, 2011). Among the functional properties of the

fibers, type I displays the slowest contraction, while types IIA, IIX, and IIB exhibit successively faster contraction (Weiss *et al.*, 1999; Goodman *et al.*, 2012). According to their morphology, the type IIB fiber is the largest and the type I fiber is the smallest. In addition to these representative fibers, other fiber types that express multiple types of MYH or minor types of MYH have been identified (Gorza, 1990; DeNardi *et al.*, 1993).

Muscle activities, such as contraction and relaxation, depend primarily on energy derived from hydrolysis of adenosine triphosphate (ATP). In order to maintain the constant supply of ATP, several metabolic processes work in muscle fibers. Those processes include glycolysis, TCA cycle, oxidative phosphorylation, creatine kinase reaction, purine nucleotide cycle, lipid metabolism, *etc*. As a characteristic feature of energy metabolism in skeletal muscles, it has been discussed that glycolysis and oxidative phosphorylation are preferentially functioning under anaerobic (fast-moving) and aerobic (resting) conditions, respectively (Westerblad *et al.*, 2010; Hargreaves & Spriet, 2020).

Each type of muscle fibers has a different preference for producing energy. The type IIB fiber exhibits the highest glycolytic activity, whereas the type I fiber exhibits the highest oxidative capacity. In relation to functional differences between fiber types, the differences in energy metabolism and the differential ATPase activities of myosin heavy chains have been studied (Haizlip *et al.*, 2015; Rosa-Caldwell & Greene, 2019). However, the exact mechanism to induce the differential metabolism among the muscle

fiber types is unknown. Furthermore, as far as I know, there is no study to determine whether there are sex differences in energy metabolism among the muscles (Comment 2).

The sexually dimorphic characteristics of skeletal muscles have been investigated extensively. The total mass of muscle fibers and their individual sizes, fiber type composition, and skeletal muscle energy metabolism, contractility, and fatigability were found to be different between the two sexes (Haizlip *et al.*, 2015; Wüst *et al.*, 2008; Hunter, 2016). For example, the female mouse masseter muscle contains fewer type IIB fibers and higher type IIA fibers than males (Eason *et al.*, 2000). The difference of the fiber type composition between the two sexes has been discussed to be correlated to slower contractile speed of females than males, and at the same time, related to a less fatigable feature of females than males (Wüst *et al.*, 2008; Hunter, 2016). Furthermore, the preferred fuels for energy metabolism have been demonstrated to be glucose and fatty acids in the muscles of males and females, respectively (Green *et al.*, 1984; Maher *et al.*, 2010). Despite the fact that these differences are thought to play a fundamental role in the sexually dimorphic functions of skeletal muscle, the mechanisms responsible for causing the features remain unknown. As described above, each type of fiber has its own preference for energy production. However, the potential contribution by the fiber types to the sexually different energy metabolism of skeletal muscles is yet unknown. Therefore, it is suggested that the sexually dimorphic glycolytic capacity can be related

to higher content of type II fibers in men (Lundsgaard & Kiens, 2014) (Comment 2). A recent study of deep sequencing revealed that skeletal muscles exhibit sexually dimorphic gene expression, in addition to morphological, physiological, and biochemical studies (Yoshioka *et al.*, 2006; Yoshioka *et al.*, 2007; Welle *et al.*, 2008; Haren *et al.*, 2011).

The role of the sex steroids have been investigated as the primary mechanism underlying sex differences (Haizlip *et al.*, 2015; Glenmark *et al.*, 2004; Aizawa *et al.*, 2008). Their roles have been defined traditionally in reproductive processes. The major sex hormones produced by the ovary are estradiol and progesterone, while that by the testis is mainly testosterone. These sex steroids are secreted into the blood flow and transferred to various tissues/cells. The hypothalamic-pituitary-gonadal axis is the central regulatory system for the reproductive activity through production of hormones: sex steroids by the gonads, luteinizing hormone (LH) and follicle stimulating hormone (FSH) by the pituitary, and gonadotropin releasing hormone by the hypothalamus. LH and FSH strictly regulate the production of sex hormones, and in turn the sex steroids give feedback effects to the hypothalamus and pituitary to control their hormone productions (Wierman, 2007).

Several male-specific characteristics of skeletal muscles, such as heavier muscle weight and larger fiber size, were shown to be the result of testosterone (Axell *et al.*, 2006; Sinha-Hikim *et al.*, 2006). Testosterone acts by binding to the androgen receptor

(AR/NR3C4), thus modulating the expression of target genes. A number of genes whose functions are closely related to the male-biased anabolic activity of muscles were shown to be targets of AR (Lee & Maclean, 2011; Rana *et al.*, 2014; Rana *et al.*, 2016). As for the action of estrogen, it has been discussed that the female hormone may potentially influence the muscle contractile properties and attenuate indices of post-exercise muscle damage. Furthermore, estrogen has been indicated to play a role in stimulating muscle repair and regenerative processes, such as the activation of function and proliferation of satellite cells. Consistent with it, adverse outcomes, such as increasing incidence of injury and delaying the recovery from it, increase in menopause women, in whom the estrogen is declining (Enns & Tiidus, 2010). Similar to androgen, estrogen binds to its cognate receptors, the estrogen receptor (ER) α (ESR1/NR3A1) and β (ESR2/NR3A2), then regulate the expression of target genes (Chidi-Ogbulu & Baar, 2019). Although many research already revealed the effect of sex steroids on the functions of skeletal muscles, the mechanism how sex steroids regulate energy metabolism in skeletal muscles remains unclear (Comment 2).

Skeletal muscles have been studied extensively and many studies have improved our understanding of their functions. Unfortunately, however, most of this research was conducted with whole muscle rather than with specific fiber types. Considering that the skeletal muscle consists of multiple fiber types, investigation of each type is thought to be essential for the overall comprehension of the functional properties of skeletal

muscle. Therefore, in the current study, I aimed to investigate sexual dimorphisms of skeletal muscle at the level of particular fiber types. My analyses of transcriptome datasets revealed that two key genes underlie sexually dimorphic metabolism. Male-predominant glycolysis was found to be due to male-enriched expression of *Pfkfb3* (phosphofructokinase-2), while female-predominant fatty acid β-oxidation was found to be due to E2 (estradiol)-enhanced expression of *Pdk4* (pyruvate dehydrogenase kinase 4).

MATERIALS AND METHODS

Operation and treatment of animals

At 3 weeks after birth, male and female C57BL/6J mice (Japan SLC, Inc.) were gonadectomized or sham operated. Bilateral ovariectomy was performed under anesthetic condition by dorsal incision at the lower back, directly below the bottom of the rib cage. Blunt forceps was used to gently free the subcutaneous connective tissue from the muscle. After founding the ovary under the thin muscle layer, small incision was made on each side to enter peritoneal cavity. For sham operation, ovarian pad surrounding the ovaries was retracted with blunt forceps to expose oviduct, and then the ovaries were replaced into the abdominal cavity. For ovariectomy mice, single ligature around the oviduct was performed to prevent bleeding following ovary removement. Ovary was gently removed. The uterus and the remaining part of the oviduct were returned into the abdominal cavity. Back incision was closed by using surgery clip (Idris, 2012).

Castration was performed as described by Valkenburg *et al.* (2016) with some modification. Vertical incision was made through the skin in the midline of the lower abdomen, approximately 1.5 cm anterior to the penis and gently free the subcutaneous connective tissue from the muscle. Small incision was made through the peritoneum, reach into the peritoneal cavity, and grip the testicular fat pad, lateral to the bladder. Fat pad was pulled through the opening until testes comes out and put back the testis into

the cavity for the sham operation. Single ligature around vas deferens was made to prevent bleeding after testes removal. Testes was gently removed, and the remaining parts were put back into the cavity. Abdominal incision was closed by surgery clip.

Three mice were housed together and fed with a standard CRF-1 chow (Oriental Yeast Co., Ltd., Tokyo, Japan). They were not exposed to the individuals of opposite sexes. The treatment with DHT and E2 was performed as shown in Figure 1. Every experimental group consisted of three male and three female mice. Skeletal muscles (gastrocnemius, tibialis anterior, quadriceps, triceps, and soleus) were isolated at eight weeks after birth and then used for further studies. A vaginal smear test was conducted to determine estrus cycle phases in females (Nelson *et al.*, 1982). All procedures involving animal experiment have been approved by the Animal Care and Use Committee of Kyushu University. All experiments were conducted in accordance with the guidelines.

mRNA sequencing and data processing

The quadriceps muscles isolated from the previously mentioned mice were immersed in RNAlater (Qiagen, Venlo, The Netherlands). Approximately 100 individual fibers were isolated from the muscles of 10 experimental groups (sham-operated male (n=3) and female mice (n=3) (CTR), pellet implantation male (n=3) (Cas+P) and female mice (n=3) (Ovx+P) after gonadectomy, oil injection male (n=3)

(Cas+Oil) and female mice (n=3) (Ovx+Oil) after gonadectomy, DHT-treated male mice (n=3) (Cas+DHT) and female mice (n=3) (Ovx+DHT) after gonadectomy, and E2-treated male mice (n=3) (Cas+E2) and female mice (n=3) (Ovx+E2) after gonadectomy) (Figure 1) using fine forceps under a SMZ-U Zoom 1:10 stereo microscope (Nikon, Tokyo, Japan) (Murach *et al.,* 2014). RNA was extracted from each fiber individually using TRIzol (Thermo Fisher Scientific, Waltham, MA, USA). cDNA was prepared from a small aliquot of each RNA sample and then subjected to PCR to determine fiber types using primer sets for myosin heavy chains (Table 2). Following the collection of RNA from type IIB fibers, ribosomal RNA was removed using a NEBNext rRNA Depletion Kit (NEB, Ipswich, MA, USA). A NEBNext Ultra II RNA Directional Library Prep Kit (NEB) was used to prepare cDNA libraries for mRNA sequencing. After the validation of quality of the cDNA libraries was conducted with an Agilent Bioanalyzer 2100 (Agilent Technologies, Santa Clara, CA, USA), the libraries were subjected to sequencing (NovaSeq 6000 System: Illumina, San Diego, CA, USA). For alignment and assembly of the sequence reads, I used STAR (version 2.7.3a) (Dobin *et al.*, 2013) and featureCounts (version 2.0.0) (Yang *et al.*, 2014), respectively. I used *Mus musculus* genome assembly (mm10, NCBI) as the reference.

qRT-PCR analysis

In this study, three biologically independent samples were used for quantitative RT-PCR (qRT-PCR). cDNAs were synthesized from total RNA by using Moloney Murine Leukemia Virus (M-MLV) reverse transcriptase (Thermo Fisher Scientific) and random primers (Sigma Aldrich). qRT-PCR was performed with a CFX96 real-time PCR system (Bio-Rad, Hercules, CA, USA) and SYBR Select Master Mix (Thermo Fisher Scientific). The primer sets used are summarized in Table 2. *Actb* (β-actin) was used to standardize the data, and it is presented as means ± standard deviation (SD). Statistical analysis was conducted by one-way ANOVA followed by the post hoc Tukey HSD test (Kitajima, S. *et al.*, 2015) or the Student's t-test. Significant differences ($p<0.01$) are shown in the figures.

Immunofluorescence analysis and CSA measurement

Immunofluorescence was performed on cryosections of the muscles of eight experimental groups (sham-operated male (n=3) and female mice (n=3) (CTR), gonadectomized mice (Cas for males (n=3) and Ovx for females (n=3)), DHT-treated male mice (n=3) (Cas+DHT) and female mice (n=3) (Ovx+DHT) after gonadectomy, and E2-treated male mice (n=3) (Cas+E2) and female mice (n=3) (Ovx+E2) after gonadectomy) (Figure 1). Immunofluorescence was performed based on previous studies with some modification (Kumar *et al.*, 2015; Quiroga *et al.*, 2016; Sawano *et al.*,

2016). Isolated skeletal muscles were placed immediately in a cryodish containing OCT-compound (SAKURA, Tokyo, Japan), and snap frozen in isopropanol that previously cooled with liquid nitrogen. Skeletal muscle block was cut as ten micrometer sections and then collected onto Matsunami adhesive silane (MAS)-coated glass slide (S9226; Matsunami Glass Ind., Ltd., Osaka, Japan). They were stored at -30°C until use.

The slides attaching tissue sections were warmed on hot plate at 37ºC overnight and washed with phosphate buffered saline (PBS) three times. After washing, the slides were steamed in 10 mM sodium citrated (pH 6.0) by a food steamer (SP-4138W; Twinbird Corporation, Tsubame City, Japan). After they were allowed to cool, the slides were incubated in PBS containing 1% Triton X-100 at room temperature for 10 min. Subsequently, the sections were incubated with Blocking One Histo (Nacalai Tesque, Kyoto, Japan) at room temperature for 20 min, and then with the primary antibodies at 4ºC overnight. After the incubation, the sections were washed with Tris-buffered saline containing 0.1% Tween 20 (TBS-T) three times and incubated with secondary antibodies at room temperature for 1 h.

In this study, I used antibodies against MYH2B (myosin heavy chain type IIB) (1:1000), MYH2A (myosin heavy chain type IIA) (1:1000) (Sawano *et al.*, 2016), and laminin (1:1000) (Sigma-Aldrich, St. Louis, MO, USA) as the primary antibodies, whereas Mouse Anti-Rat IgG2b-Alexa Fluor® 647 (1:500, SouthernBiotech,

Birmingham, AL, USA), Mouse Anti-Rat IgG1-Alexa Fluor 488® (1:500, SouthernBiotech), and Alexa Fluor 488-labeled Goat Anti-Rabbit IgG (1:500, Thermo Fisher Scientific) were used as the secondary antibodies. The nuclei were stained with 4',6'-diamidino-2-phenylindole (DAPI) (Sigma-Aldrich). According to the manufacturing protocol, All antibodies were diluted with mix solution of TBS-T and Blocking One Histo. An LSM 700 confocal laser scanning microscope (Zeiss, Oberkochen, Germany) was used to observe the fluorescence signal. An analysis of histological images was performed using ImageJ software (Fiji) (Schindelin *et al.*, 2012) to determine the CSAs of the muscle fibers. Accordingly, the average number of fibers examined in the sham-operated males and females, gonadectomized males (Cas) and females (Ovx), DHT-treated males (Cas+DHT) and females (Ovx+DHT) after gonadectomy, and E2-treated males (Cas+E2) and females (Ovx+E2) after gonadectomy are presented in corresponding order for each muscle as follows: for the quadriceps, 4800, 7500, 5900, 5100, 5500, 4900, 4900, and 6200 fibers, respectively; for the tibialis anterior, 2500, 2300, 3600, 3100, 4000, 3200, 3300, and 3300 fibers, respectively; for the gastrocnemius, 5900, 4600, 5700, 5400, 6200, 5100, 6700, and 4100 fibers, respectively; for the triceps, 4500, 4300, 4800, 4200, 5200, 4200, 4800, and 4300 fibers, respectively; and for the soleus, 50, 55, 65, 40, 65, 50, 63, 40 fibers, respectively. The CSAs data are presented as means ± SD and were analyzed

statistically by one-way ANOVA followed by the post hoc Tukey HSD test or the Student's t-test.

Preparation of muscle fibers from quadriceps muscle

Type IIB fiber-enriched areas in quadriceps muscles were identified by an immunofluorescence study. In these areas, approximately over 95% fibers were type IIB. Living muscle fibers were prepared from the areas and cultured as described previously (Pasut *et al.*, 2013; Kitajima *et al.*, 2016; Hüttner *et al.*, 2019). The regions isolated from eight quadriceps muscles were incubated with 4 mg collagenase type I (Worthington Industries, Columbus, OH, USA) in 2 ml Dulbecco's Modified Eagle Medium (DMEM, Thermo Fisher Scientific) at 37°C under 5% CO_2 for 1.5 h with gentle shaking by hand every 15 min. Petri dish coated with fetal bovine serum (FBS) (Thermo Fisher Scientific) to prevent myofibers from adhering were filled with warmed DMEM. The muscles were dissociated into individual myofibers using Pasteur pipette having a hole with a larger diameter. The pipettes were rinsed previously with FBS to flush the muscle until the fibers released spontaneously. This procedure was performed under stereo microscope. The process above was repeated until the fibers enough for experiments were obtained. If the process required to put the dish contained muscle at room temperature for more than 10 min, the dish was put back to the incubator for 5 min to re-equilibrate the medium.

Single live myofibers was transferred to new prewarmed dish containing DMEM. The dish was incubated for at least one hour before switching the culture medium to DMEM supplemented with 20% FBS, 2% chick embryo extract (United States Biological, Salem, MA, USA), and 1% penicillin-streptomycin (PS, 10,000 U/ml, Thermo Fisher Scientific). Over 80% of the recovered fibers remained alive after overnight incubation. A microscopic examination was conducted in order to assess the viability of the isolated muscle fibers. Generally, healthy muscle fibers are long, translucent, and have clear surfaces without any shears, as described previously (Pasut *et al.*, 2013; Hüttner *et al.*, 2019; Gallot *et al.*, 2016).

Knockdown of Pfkfb3 and Pdk4

One hundred fibers prepared above were cultured on a plate coated with Matrigel matrix (Corning Incorporated, Corning, NY, USA) with 500 μl standard medium (DMEM containing 25 mM glucose supplemented with 20% fetal bovine serum (Thermo Fisher Scientific), 2% chick embryo extract (United States Biological), and 1% penicillin-streptomycin (PS, 10,000 U/ml, Thermo Fisher Scientific) at 37°C under 5% CO_2 for 24 h. A mixture of two *Pfkfb3* small interfering RNA (siRNA) duplexes (si*Pfkfb3*, 200 nM, SASI_Mm01_00034119 and SASI_Mm01_00034121 (Sigma-Aldrich)) or two *Pdk4* siRNA duplexes (si*Pdk4*, 100 nM, SASI_Mm01_00053023 and SASI_Mm01_00053024 (Sigma-Aldrich)) were transfected into the fibers using

Lipofectamine RNAiMAX (Thermo Fisher Scientific) for 6, 9, 12, or 24 h in standard medium without PS. Stealth RNAi^{TM} siRNA Negative Control, Med GC (Thermo Fisher Scientific) was used as a negative control. Transfection was performed according to the manufacturer's protocol and the procedure described by Huttner *et al*. (2019). RNAs were prepared from the fibers and then subjected to qRT-PCR of *Pfkfb3* and *Pdk4*.

Extracellular acidification rate (ECAR) measurement

The ECAR was measured in accordance with the manufacturer's specifications using the Seahorse XFe96 Analyzer (Agilent Technologies). Fifteen muscle fibers were plated on a 96-well plate (Agilent Technologies), which was precoated with Matrigel matrix (Corning Incorporated). They were incubated with 200 μl of standard medium for 18 h, then cultured in XF base medium (Agilent Technologies) supplemented with 2 mM glutamine (Agilent Technologies) for 1 h at 37°C without CO_2. After the addition of 2 mM glucose, the ECAR was measured.

In order to evaluate the effect of *Pfkfb3* knockdown, muscle fibers were transfected with si*Pfkfb3* for 6 h after 18-h culture in standard medium. Following transfection, the fibers were further cultured in standard medium for another 12 or 24 h. They were subjected to ECAR measurement after 1-h culture in XF base medium. In general, approximately 10% of the fibers died during the transfection, and the numbers of living

fibers varied among wells. Therefore, ECAR measurement were performed only on the wells containing at least living 13 fibers at the end of the transfection. As fiber size differed between males and females, the amount of protein in each fiber was examined (Table 10) and ECARs were corrected using the ratio of the mean protein content in the fibers of the two sexes (male/female = 1.10). I used three biologically independent samples. The ECAR data are presented as means ± SD and were analyzed by one-way ANOVA followed by the post hoc Tukey HSD test or the Student's t-test.

Oxygen consumption rate (OCR) measurement

A seahorse XFe96 Analyzer (Agilent Technologies) was used to measure OCR, in accordance with the manufacturer's protocol. In total, fifteen muscle fibers were prepared from each of the following groups: male mice (n=3), oil-injected female mice in diestrus (n=3), and female mice treated with E2 for 24 h (n=3). All fibers were placed on a 96-well plate precoated with Matrigel matrix (Corning Incorporated) and incubated in 200 μl of standard medium for 18 h. The medium was changed to XF base medium supplemented with 1 mM pyruvate, 2 mM glutamine, and 10 mM glucose, and the muscle fibers were incubated for 1 h without CO_2 before the OCR measurement. The fatty acid-dependent OCR was measured using 4 μM Etomoxir (Seahorse XF Mito Fuel Flex Test Kit, Agilent Technologies) as an inhibitor of carnitine palmitoyl-transferase.

The amount by which the OCR was decreased by the inhibitor was defined as the fatty acid-dependent OCR.

To investigate the effect of Pdk4 knockdown, fibers were transfected with siPdk4 or control siRNA after 18-h incubation in standard medium. Following transfection, wells containing at least 13 living fibers were used for OCR measurement. Simillar to the ECAR measurements, the OCRs of fibers from males and females were corrected by the ratio of the mean protein content in the fibers of the two sexes (male/female = 1.10) (Table 10). Three biologically independent samples were for the analyses. The OCR data are presented as means ± SD and were analyzed using one-way ANOVA followed by the post hoc Tukey HSD test.

Western blotting

Whole protein lysate was isolated from the type IIB fiber-enriched area in quadriceps muscles. The fibers were lysed using radioimmunoprecipitation assay (RIPA) buffer (Sigma-Aldrich), followed by sonication (Branson Ultrasonics^{TM} S-250A Model Sonifier^{TM} Analog Cell Disrupter, Branson, Brookfield, CT, USA). This procedure was performed to obtain proteins for PFKFB3 western blotting analysis.

Mitochondria were isolated from the muscle fibers as described by Garcia-Cazarin *et al.* (2011), and then used to detect PDK4, PDH, and P-PDH. In brief, skeletal muscle was isolated, rinsed in ice-cold PBS, and rinsed again in ice-cold PBS-EDTA (PBS with

10 mM EDTA). After the muscles were transferred to the tube containing isolation buffer and then minced with scissors, they were homogenized with Potter-Elvehjem homogenizer with 10 times of strokes while keeping the tube on ice. After a series of centrifugation and washing, the pellet containing isolated mitochondria were resuspended in a buffer containing 3 mM EGTA, 215 mM D-mannitol, 0.6 M Sucrose, 0.8 % Bovine Serum Albumin (BSA), 160 mM HEPES.

The protein concentration was examined using BCA Protein Assay Kit (Thermo Fisher Scientific). 30 μg whole lysate or 10 μg mitochondrial proteins were subjected to sodium dodecyl sulfate (SDS)-polyacrylamide gel electrophoresis, followed by western blotting. I used anti-PFKFB3 (1:2000, Proteintech, Rosemont, IL, USA), anti-GAPDH (1:10000, Santa Cruz Biotechnology, Dallas, Texas, USA), anti-PDK4 (1:1000, Proteintech), anti-PDH (1:1000, Cell Signaling Technology, Danvers, MA, USA), anti-phospho-PDH α1 (1:1000, Cell Signaling Technology), and anti-COXIV antibodies (1:2000, Abcam, Cambridge) as primary antibodies. As secondary antibody, HRP labeled anti-mouse IgG (Goat), (1:2000, Thermo Fisher Scientific) and HRP-linked F(ab')2 fragment of anti-Rabbit IgG, (Donkey) (1:2000. Cytiva, Marlborough, MA, USA) were used. I performed semi quantification of the proteins detected by western blotting using ImageJ software (Fiji) (Schindelin *et al.,* 2012). Data (means ± SD) obtained from three biologically independent samples were analyzed by one-way ANOVA followed by the post hoc Tukey HSD test or the Student's t-test.

Statistics and reproducibility

Student's t-test was used to calculate statistically significant differences between two groups. The significant differences between multiple groups were assessed using one-way ANOVA followed by the post hoc Tukey HSD test. Three biologically independent samples were used in each experiment.

RESULTS

Effect of gonadectomy and hormone replacement on skeletal muscle

To evaluate the effect of sex hormones and chromosomes on skeletal muscle, mice were gonadectomized and treated with hormones. The mice were sacrificed at the end of the treatment period (Figure 1). The weights of the seminal vesicle in male and that of the uterus in female were decreased after gonadectomy, and subsequent the hormone replacement treatment (HRT) rescued the weights of both organs (Figure 2a), suggesting that the experimental treatments effectively worked.

Pellet implantation and subcutaneous injection were used for DHT and E2 replacement, respectively. The DHT concentration is 5 mg/pellet/mouse. The concentration of the injected E2 was 500 μg/kg body weight based on the previous studies (Padilla-Banks et al., 2001; Laredo et al., 2013; Safari et al., 2015; Ghobadi, 2016). In order to mimic intrinsic estrus cycle of mice, the E2 injection was performed every four days, similar to the study by Corculio et al. (2021). The uterus weight was found to be increased by the E2 injection, as compared to those of the ovariectomized mice with vehicle injection (Figure 2a). No significant difference was found between the E2-injected and the sham-operated control mice. Bodyweight was slightly but not significantly increased by the E2 treatment. These results were consistent with those obtained by other studies (Padilla-Banks et al., 2001; Safari et al., 2015; Corculio et al., 2021). No significant difference was found in the weight of quadriceps muscles when

the muscles were compared between the E2-injected and the sham-operated control mice (Figure 2b) (Comment 4).

Five skeletal muscles (quadriceps, tibialis anterior, gastrocnemius, triceps, and soleus) were isolated and weighted. The male skeletal muscles tend to develop higher mass compared to female. The weights of the five muscles showed differential responses to the treatments (Figure 2b). All muscles showed similar responses to a DHT (dihydrotestosterone) treatment, resulting in an increase of the muscle weights in both male and female.

Sexual dimorphism seen in skeletal muscle fibers size

Several sexually dimorphic features present in skeletal muscles have been reported. I attempted to confirm the sexual dimorphism seen in muscle fiber size (cross-sectional area (CSA)) using the five different skeletal muscles (quadriceps, tibialis anterior, gastrocnemius, triceps, and soleus) of 8-week-old male and female mice (Figure 3a). In all skeletal muscles examined, the fiber CSAs were larger in males than females (Figure 3b), although the male to female ratios were varied among the skeletal muscles.

Mammalian skeletal muscles consist of four types of muscle fibers according to the type of myosin heavy chain expressed: type I, IIA, IIB, and IIX fibers, that can be distinguished by the predominant expression of *MYH7* (encoding MYH1), *MYH2* (encoding MYH2A), *MYH4* (encoding MYH2B), and *MYH1* (encoding MYH2X),

respectively (Schiaffino & Reggiani, 2011; Berchtold *et al.,* 2000; Wang *et al.,* 2012). To investigate the fast fiber's composition among five skeletal muscle area, antibodies to MYH2A and MYH2B were used for identification of type IIA and IIB fibers (a major fast fiber type in fast-twitch skeletal muscles in rodents), respectively (Figure 4a). Fast-twitch muscles such as tibialis anterior, gastrocnemius, quadriceps and triceps muscles were dominated with MYH2B-positive type IIB fast fibers. By contrast, slow-twitch soleus muscle was dominated with MYH2A-positive type IIA fast fibers together with unstained fibers (possibly types I and IIX). In the skeletal muscles investigated, the CSAs of type IIB fibers were larger in males than females (Figure 4b). I focused on this fiber type in the following studies to further investigate the sexually dimorphism in CSA.

The next question I addressed was when the sex difference emerges in the skeletal muscles. Postnatally, the CSAs of quadriceps type IIB fibers were examined at 2, 3, 4, and 8 weeks (Figure 5a). A slight difference between sexes was evident at 4 weeks, and the difference became more pronounced at 8 weeks. *Amd* (S-adenosylmethionine decarboxylase) and *Smox* (spermine oxidase), both of which are required for polyamine synthesis, have been reported to exhibit male-enriched and androgen-induced expression (Yoshioka *et al.*, 2006; Yoshioka *et al.*, 2007; Haren *et al.*, 2011; Sakakibara *et al.*, 2021). The expressions of these genes were assessed in quadriceps type IIB

fibers. Similar to the CSAs, I also observed slight male-enriched expressions at 4 weeks and were clearly apparent at 8 weeks (Figure 5b).

Effect of sex steroids on skeletal muscle fibers size

To investigate the effect of sex steroids on CSAs, I prepared muscles from sham-operated males and females, castrated males (Cas), ovariectomized females (Ovx), mice treated with DHT (dihydrotestosterone) after gonadectomy (Cas+DHT and Ovx+DHT), and mice treated with E2 after gonadectomy (Cas+E2 and Ovx+E2). Before the muscles show sex difference, mice were gonadectomized at 3-week, and then they were transplanted with a DHT-containing pellet or injected with E2 (Figure 1). Of note, as the control female, I used diestrus mice that had undergone sham operation.

After the muscle cross-sections were stained with antibodies to MYH2A and MYH2B, the CSAs of the MYH2B-positive type IIB fibers were measured. Immunofluorescence analysis suggested that type IIB fibers were larger in males than in females, and the sizes were changed by gonadectomy and the following sex hormone treatments (Figure 6a, b). Statistical analyses revealed that the CSAs of the quadriceps, tibialis anterior, triceps, and soleus were larger in males than in females (Figure 6c). With a few exceptions, DHT generally increased the CSAs of the muscles above regardless of sex. However, E2 did not increase CSAs.

The type IIB fiber sizes in the quadriceps, tibia anterior, triceps, and soleus showed sexual dimorphism: larger in male than female. Castration decreased the CSA, and ovariectomy did not show any effect on it. DHT treatment after gonadectomy enlarged the CSA in male muscles except soleus. Similarly, the treatment enlarged it in the quadriceps of female, while other female muscles were presumably enlarged at moderate levels. E2-treatment after ovariectomy did not seem to give any significant effect on the CSAs of the female muscles. These results indicated that the effects of the gonadectomy and sex steroid treatments on the type IIB fiber sizes are varied among the skeletal muscles and between the two sexes. However, consistent with the previous reports (Sinha-Hikim *et al.*, 2006; Sinha-Hikim *et al.*, 2002; Bhasin *et al.*, 2003; Dubois *et al.*, 2012; O'Connell & Wu, 2014; Morton *et al.*, 2018), my results above suggested that the male-enlarged muscle fiber size primarily depends on testosterone.

Among the responses to the sex steroids, I noticed a unique response of the quadriceps to the DHT-treatment (Figure 6a, b). Although the male and female quadriceps fibers responded to DHT, the enlarged male fibers were still larger than those of the female, suggesting that sexually dimorphic potential to respond to testosterone might be maintained intrinsically by the XY and XX chromosome in quadriceps fibers.

Sexually dimorphic gene expression in quadriceps type IIB fibers

Due to the clear sexual dimorphism and DHT dependency of the CSAs of quadriceps muscle type IIB fibers, I decided to obtain transcriptomes of these fibers. In all 10 experimental mouse groups (sham-operated males and females, males and females transplanted with a DHT-containing or empty pellet after gonadectomy, and males and females injected with E2-containing or corn oil after gonadectomy), single fibers were isolated from an area of the quadriceps where approximately 95% fibers are type IIB (Figure 7a). Indeed, RT-PCR confirmed that the fiber types are predominantly consist of type IIB (Figure 7b).

The RNAs recovered from fibers expressing MYH2B positive (encoded by *MYH4*) were pooled and subjected to mRNA sequencing. From all experimental groups above, transcriptome datasets with sufficient quality for the following analyses were obtained (Table 1). The expression of the *MYH4* was considerably higher than those of other *MYH* genes, indicating that the fibers prepared were predominantly type IIB (Table 3). The genes with CPM values (counts per million mapped reads) greater than 10.0 in either the sham-operated males or females were extracted as all expressed genes (6,978 genes) and utilized for the following analyses. Among these genes, 68 and 60 were enriched more than 2.0-fold in males and females, respectively (Figure 8a, Table 4, Table 5). As described in detail below, two key genes involved in energy metabolism,

Pdk4 (pyruvate dehydrogenase kinase 4) and *Pfkfb3* (phosphofructokinase-2), were among the male-enriched genes.

Expression profiles of the male-enriched and female-enriched genes among the 10 experimental groups were analyzed by hierarchical clustering (Figure 8b, 8c). Based on the clustering profile of the male-enriched genes, male, Cas+DHT, and Ovx+DHT mice were classified into one subgroup (Figure 8b). Almost half of the male-enriched genes exhibited DHT-dependent expression. Similarly, the effect of DHT was observed in the ovariectomized females. Interestingly, however, a part of the genes responded to DHT were differentially expressed between male and female skeletal muscle. Moreover, the expression of approximately one third of the genes were failed to be restored by the DHT treatment. Furthermore, clustering of the female-enriched genes indicated that the same experimental groups were likely to form a subgroup (Figure 8c). Comparing female, Cas+E2, and Ovx+E2 mice, we found that a number of the female-enriched genes appeared to be activated by E2 in both sexes. Despite the fact that both DHT and E2 affected gene expression, it is likely that the effects of DHT are more apparent than those of E2.

Unexpectedly, I found that a group of male-enriched genes were activated following empty pellet implantation in castrated males (Cas+P), although this phenomenon was not observed in ovariectomized females (Ovx+P). I carefully

examined the subsequent results since the cause for this unexpected gene activation by control treatment was not known.

Principal component analysis of whole transcriptome data was carried out to classify the mouse groups. Male, Cas+DHT, and Ovx+DHT mice formed a separate subgroup (SG1 in Figure 8d). It was unclear whether female, Cas+E2, and Ovx+E2 mice belonged to the same group. The experimental group, Cas+P, was classified separately from the other groups, perhaps due to the unexpected gene activation caused by the empty pellet implantation described above. Previous study reported that the testosterone levels were different among mouse strains, and that of C57BL/6 was significantly lower than those of CD-1, CH3, and FVB (Brouillette *et al.*, 2005). Studies using the mice with higher testosterone levels might provide evidence of more pronounced sexually dimorphic gene expression.

Biological functions related to male- and female-enriched genes

Gene ontology analyses were performed on the sex-biased genes. The results suggested that a variety of biological processes are more active in male type IIB fibers of quadriceps (Table 6). The polyamine biosynthetic process was identified as a potential biological process associated with the male-enriched genes. Since spermidine, one of the polyamine biosynthetic products, has been established as a potent activator for muscle fiber enlargement (Bongers *et al.*, 2015; Cervelli *et al.*, 2018; Lin *et al.*,

2018; Uchitomi *et al.*, 2019), the expression data for the polyamine synthetic genes were extracted from the transcriptome datasets of the 10 experimental groups. Among the polyamine synthetic genes, *Odc1* (ornithine decarboxylase 1), *Amd1/2*, and *Smox* showed higher expressions in males as compared with females and were induced by DHT treatment in both sexes (Figure 9). Empty pellet implantation did not result in an upregulation of the expression of these genes.

In previous studies, these polyamine synthetic genes were found to be male enriched and androgen inducible (Yoshioka *et al.*, 2006; Yoshioka *et al.*, 2007; Haren *et al.*, 2011; Sakakibara *et al.*, 2021). In relation to their function in skeletal muscles, they were reported to suppress muscle atrophy and promote hypertrophy (Bongers *et al.*, 2015; Cervelli *et al.*, 2018), possibly by modulating cellular proliferation and viability (Pendeville *et al.*, 2001; Nishimura *et al.*, 2002) as well as protein synthesis (Igarashi & Kashiwagi, 2015) and autophagy (Eisenberg *et al.*, 2008; Madeo *et al.*, 2018). In summary, it appears to be the case that differences in muscle sizes are largely determined by variations in androgen levels between males and females.

According to the gene ontology analysis, the terms “collagen fibril organization,” “wound healing,” and “skeletal system development” were associated with the female-enriched genes. Since collagen genes were commonly included in these processes, I extracted the expression data of all collagen genes from the datasets of the 10 experimental groups. As shown in Table 7, the expressions of many collagen genes

were higher in females than in males. Unlike the DHT effect on the polyamine synthetic genes, many female-enriched collagen gene expressions seemed to be affected neither by ovariectomy nor sex steroid treatments in female. By contrast, in male, the expression of these genes was induced by castration. In addition to the collagen genes, the expression profile of *Adamts2*, whose product is necessary for processing of procollagens, was similar to those of the collagen genes.

Differential regulation of Pdk4 and Pfkfb3 genes by sex steroids

Since diestrus mice with low E2 serum concentrations were used as the control females, it was assumed that a certain population of genes that might be activated by E2 would not be included in the female-enriched genes. Therefore, the E2 induction ratios for all of the expressed genes (6,978) were calculated in males and females (Cas+E2/Cas+Oil and Ovx+E2/Ovx+Oil) and are shown in Figure 10a. The accumulation of genes in the upper right and lower left quadrants indicated that numerous genes were activated and suppressed by E2 regardless of sex. Nevertheless, this pattern was not observed when only the female-enriched genes were analyzed (Figure 10b). Additionally, many genes that showed relatively high activation or suppression by E2 were excluded from the female-enriched genes. Even in female mice, Female-enriched *Col* genes were not activated intensively by E2. As a consequence, this analysis revealed E2-induced genes that did not belong to of the female-enriched gene

population. It is noteworthy that two key genes regulating energy metabolism, *Pdk4* and *Pcx* (pyruvate carboxylase), were included.

Likewise, the DHT induction ratios for all expressed genes were calculated (Figure 10c). Similar to the E2 results above, the accumulation of genes in the upper right and lower left quadrants suggested that many genes were activated and suppressed, respectively, by DHT regardless of sexes. Moreover, I examined whether the male-enriched genes potentially induced by DHT were induced similarly by the steroid also in female. Thus, the induction ratios (Cas+DHT/Cas+P) for the male-enriched genes in male were compared with those (Ovx+DHT/Ovx+P) in female. As shown in Figure 10d, the male-enriched 68 genes were plotted as the functions of DHT dependency in male (horizontal axis) and female (vertical axis). Approximately, a half of the genes is localized at the upper right and lower left quadrant, indicating that their gene expressions were increased or decreased, respectively, by DHT regardless of sexes. As expected, polyamine synthetic genes, *Smox* and *Amd1/2*, were localized in the upper right quadrant, indicating that they were activated by DHT regardless of sex. Interestingly, I found genes whose expression was activated preferentially in female (upper left) or in male (lower right). Even though *Pdk4* and *Pfkfb3* were male-enriched genes, their localizations are different from those of *Smox* and *Amd1/2*, suggesting that the expressions of *Pdk4* and *Pfkfb3* were relatively unaffected by DHT in both sexes.

Possible contribution of Pfkfb3 to male-predominant glycolysis

Many studies extensively characterized energy metabolisms preferred by the fiber types (Colliander *et al.*, 1988; Ball-Burnett *et al.*, 1991; Scott *et al.*, 2001; Zierath *et al.*, 2004; Liu *et al.*, 2015; Julien *et al.*, 2018). Among the four fiber types, fast-twitch fiber type IIB and slow-twitch fiber type I exhibit a clear contrast in the preferential utilization of anaerobic glycolysis and aerobic oxidation, respectively (Herbison *et al*., 1982). In addition, it has been established that both aerobic oxidation and anaerobic glycolysis of fast-twitch skeletal muscles is higher in male than female (Pette, 1985). These observations made me anticipated that the glycolytic activity of type IIB is higher in male than female.

In glycolysis regulation, PFKFB3 plays a crucial role by producing fructose-2,6-bisphosphate, which strongly activates PFKM (the type of phosphofructokinase-1 found in muscles) (Mulukutla *et al*., 2014; Almacellas *et al*., 2019) (Figure 11a). Thus, the male-enriched expression of *Pfkfb3* suggested that glycolytic activity in quadriceps type IIB fibers would be higher in males than in females. To examine this hypothesis, I prepared muscle fibers from a particular region (white quadriceps) (Devries, 2016) of the quadriceps (Figure 7a), and the extracellular acidification rate (ECAR), an index of glycolytic activity, was determined. In line with my expectation, the ECAR was approximately two-fold higher for muscle fibers from males than from females (Figure 11b).

I speculated that male-biased glycolytic activity might be caused by higher expressions of glycolytic genes in males as well as by the upregulated expression of *Pfkfb3*. Nevertheless, neither the transcriptome data nor qRT-PCR indicated a male-enriched expression of any glycolytic genes (Figure 11c, Table 8). In addition, their expressions were not significantly affected by gonadectomy or sex steroid treatments. On the other hand, both transcriptomic analysis and qRT-PCR (Figure 11d, 11e) indicated that *Pfkfb*3 expression was decreased significantly by castration but not by ovariectomy. Consistent with the results shown in Figure 10c and d, DHT treatment failed to reverse the expression decreased by castration, suggesting that unknown factors from the testis, solely or together with testosterone, might regulate *Pfkfb3* gene expression in male. Likewise, the DHT treatment unlikely affect the expression in female. The E2 treatment seemed to affect *Pfkfb3* gene expression to opposite directions between the two sexes, suppression in male and slight activation in female. *Pfkfb3* expression was not affected by implantation of an empty pellet. Expectedly, the male-enriched expression of PFKFB3 was observed at the protein level (Figure 11f).

Based on the results above, it strongly suggested that male-predominant glycolysis can be achieved by the male-enriched expression of *Pfkfb3* alone. To verify this, I performed a knockdown study of the gene. As the first step, I examined whether the gene could be suppressed using a general procedure for siRNA knockdown in cultured muscle fibers. These fibers were transfected with siRNAs targeting *Pfkfb3* or control

siRNA for 6, 12, or 24 h, and then the mRNA was quantified by qRT-PCR (Figure 12a). As a result of the siRNA treatment, *Pfkfb3* expression was suppressed by approximately 25% at 6 h and then to 40-50% at 12 and 24 h after the treatment. This study demonstrated that siRNA treatment potentially suppresses gene expression in the cultured muscle fibers. In addition, PFKFB3 was decreased at the protein level by the si*Pfkfb3* treatment (Figure 12b).

Therefore, under this condition, I examined whether Pfkfb3 knockdown could decrease the glycolytic activity of the type IIB muscle fibers. An examination of the ECAR under the knockdown condition demonstrated that si*Pfkfb3* treatment decreased the glycolytic activity in the male-derived muscle fibers at 12 h, with an even further suppression effect observed at 24 h (Figure 12c). Additionally, the activity of the si*Pfkfb3*-treated male-derived fibers decreased to approximately the same level as the siControl-treated female-derived fibers. In summary, these results strongly suggest that the male-predominant glycolytic activity of quadriceps type IIB fibers can be established largely by the male-enriched expression of *Pfkfb3*.

Possible contribution of Pdk4 to female-predominant fatty acid metabolism

Female skeletal muscles utilize fatty acid β-oxidation rather than glycolysis to produce energy (Green *et al*., 1984; Mahlapuu *et al*., 2004). Thus, I examined the expression of genes involved in fatty acid β-oxidation in the transcriptome datasets and

using qRT-PCR (Figure 13a, Table 9). While most of these genes showed a tendency to be activated by E2, none of them displayed female-enriched or E2-enhanced expression over twice the baseline level. In contrast, the transcriptome data demonstrated E2-enhanced expression of *Pdk4*, which was further confirmed by qRT-PCR (Figure 10a, Figure 13b, c). As well as the level of mRNA, PDK4 was also increased in the E2-treated female muscle fibers at the protein level (Figure 13d).

In terms of its function, it has been established that PDK4 promotes the utilization of fatty acids as a source of energy by suppressing the pyruvate dehydrogenase complex through phosphorylation (Pettersen *et al*., 2019) (Figure 16). Accordingly, the phosphorylation level of PDH (P-PDH) increased significantly in the E2-treated female muscle (Figure 13d). Therefore, I hypothesized that female-predominant fatty acid β-oxidation could be caused by E2-induced *Pdk4*. To investigate this, I examined the fatty acid-dependent oxygen consumption rate (OCR) using cultured muscle fibers from male mice and diestrus female mice treated with or without E2 for 24 h. The result of this experiment was presented in Figure 14a. The fatty acid-dependent OCR was similar between male mice and diestrus female mice. The OCR was enhanced two-fold by E2 treatment, as expected. Regarding the effect of E2 on female metabolism, we also measure glucose-dependent (Figure 14b) and glutamine-dependent (Figure 14c) OCR with E2-treated female muscle fibers. The results shown in Figure 14 indicated that E2 did not affect the level of dependency of both glucose and glutamine in females.

Lastly, I examined the effect of *Pdk4* knockdown. As a result of si*Pdk4* treatment of muscle fibers, the amount of *Pdk4* mRNA was decreased to 40% by 6-h treatment, and to 20% by 9- and 12-h treatments (Figure 15a). This is consistent with the level of PDK4 protein decreased following the si*Pdk4* treatment (Figure 15b). I then examined whether phosphorylation level of PDH is decreased by the si*Pdk4* treatment. Accordingly, it was found that the phosphorylation levels of PDH in the E2-treated female and male were significantly reduced (Figure 15c). Furthermore, muscle fibers treated with siRNA for 9-h were subjected to the aforementioned OCR assay. *Pdk4* knockdown resulted in a reduce of fatty acid-dependent OCR across samples. Intriguingly, the enhancement of fatty acid dependency caused by E2 treatment was nullified by *Pdk4* knockdown (Figure 15d). Overall, these results strongly suggest that female-predominant fatty acid utilization is attributable to E2-induced *Pdk4* gene expression.

Discussion

Effect of gonadectomy and DHT treatment on skeletal muscle weight

Gonadectomy affects the weight of reproductive organ such as uterus in female and seminal vesicle in male mice (Wakley *et al*., 2016). Seminal vesicle is originated from Wolffian ducts, and its development is known to be controlled by DHT (Shima *et al*., 1990). Meanwhile, the uterus is originated form the Müllerian ducts (Hassan *et al*., 2010; Behr *et al*., 2012; Robbins *et al*., 2015). After differentiation of functional epithelial tissues, they become estrogen-dependent (Alderman & Taylor, 2021). Castration and ovariectomy decrease the level of testosterone and estrogen, and as a consequence, decrease the weight of seminal vesicle and uterus, respectively (Quarmby *et al*., 1984; Tian *et al*., 2015). Therefore, uterus or seminal vesicle weight is known to be the indicator for hormonal change after castration, ovariectomy, and/or hormone replacement (Cabral *et al*., 1988; Erben *et al*., 2002; Raudrant *et al*., 2003; Fitts *et al*., 2004).

In general, hormone replacement therapy with DHT showed a tendency to increase skeletal muscle weight in male and female (Figure 2b). DHT is the active form of testosterone, one of the major androgens in male (Horton & Tait, 1967). Androgens are known to give effects on protein, carbohydrate, and fat metabolism and therefore contribute to determination of muscle mass and strength (Marin *et al*., 1992; Urban *et al*., 1995; Kohn, 2006). Increase of muscle mass occurs during puberty as a result from

the increasing of testosterone. The mechanism of action has been attributable to increase of satellite cells, which in turn promotes protein synthesis (Brown, 2008). The effect of androgens in muscle is dose dependent (Zitzmann & Nieschlag, 2001) and may be fiber type specific. However, it is unclear whether androgens affect both fast- or slow- twitch muscle (Sinha-Hikim *et al*., 2002; Axell *et al*., 2006; Hulmi *et al*., 2008; Ophoff *et al*., 2009). Therefore, in our study, several skeletal muscles were investigated. Eventually, it was shown that every skeletal muscle were increased by the DHT treatment in both sexes.

Emergence of sexual dimorphism in skeletal muscle CSA

Previous study by Bachman *et al*. (2018) showed that myofiber size in mice was significantly increased during pubertal age. During this period, one of the pivotal points is the reduction of Satellite cells (SC) that contribute to the developing myofiber. Sex hormones (both androgens and estrogens) can induce Notch signaling in cycling SC and convert it to their adult quiescent state (Kim *et al*., 2016). In agreement with those studies, a significant difference of the CSA of male and female muscles was observed from four weeks after birth, and more profound at eight weeks old (Figure 5).

Testosterone is one of the factors to induce sexually different myofiber sizes. Testosterone is an anabolic hormone that controls the muscle protein balance by enhancing protein synthesis and improving amino acid reutilization (Sipila *et al*., 2013).

The increasing level of testosterone during prepubertal to pubertal period stimulates muscle protein synthesis (Brown, 2008), and therefore this testosterone dependent increase might contribute to the differential muscle fiber sizes between male and female. As described previously, DHT treatment tends to increase the skeletal muscle weight and it is partly due to increasing CSA of both type I and type II muscle fibers (Sipila *et al*., 2013).

Male-predominant glycolysis due to male-enriched expression of Pfkfb3

There have been numerous transcriptome datasets collected from skeletal muscles to evaluate the effects of exercise, metabolic diseases, aging, etc (Lin *et* al., 2018; Melouane *et al*., 2018; Pillon *et al*., 2020). In some of them, sexually dimorphic gene expression was discovered, while others demonstrated the effects of sex steroids (Yoshioka *et al*., 2006; Yoshioka *et al*., 2007; Welle *et al*., 2008; Haren *et al*., 2011). In addition to these transcriptome analyses, many studies have characterized the sexually dimorphic structures and functions of skeletal muscles (Haizlip *et al*., 2015). One fundamental difference in energy metabolism between male and female can be attributed to the fact that male skeletal muscles preferentially utilize glycolysis, while female muscles tend to rely on mitochondrial fatty acid β-oxidation (Rosa-Caldwell Greene, 2019). In addition, it was also shown, regardless of sex, that the main type of metabolism in some skeletal muscle fibers is anaerobic glycolysis, while in others it is

aerobic mitochondrial oxidation (Herbison *et al*., 1982). Thus, the sexual dimorphism in the energy metabolism of skeletal muscle can be explained by the predominance of glycolytic fibers in males and of oxidative fibers in females. However, it is also possible that sexually dimorphic metabolism can be explained by differential metabolic activities intrinsic to male and female fibers. In order to investigate this issue, in this study, I focused on type IIB fibers, which are the most abundant type of fiber in fast-twitch muscles in rodents (Hamalainen & Pette, 1993; Augusto *et al*., 2004).

Based on the result obtained by my study, I found that male-predominant glycolytic activity could not be accounted for simply by enhanced glycolytic gene expression in males. Interestingly, however, *Pfkfb3* was identified as one of the male-enriched genes in this study. PFKFB3 is involved in converting F-6-P (fructose-6-phosphate) into F-2,6-BP (fructose-2,6-bisphosphate), the latter of which functions as a potent allosteric activator of PFKM (a muscle type of PFK-1), one of the glycolytic rate-limiting enzymes (Van Schaftingen *et al*., 1980). During supramaximal exercise, activated glycolysis leads to increased lactate concentrations, causing the pH of muscle fibers to become acidic, and simultaneously causes rapid reductions in oxygen and glucose concentrations (Jacobs *et al*., 1983). As a consequence, these conditions are known to decrease glycolytic activity by inhibiting the action of PFKM. Intriguingly, however, suppression of the liver type of the PFK-1 can be released by the robust action of F-2,6-BP, which is produced by PFKFB3 (Wu *et al*., 2006; Yalcin *et al*., 2009; Rovira *et al*.,

2012). Considering that the concentration of F-2,6-BP was shown to be correlated with the expression level of *Pfkfb3*/PFKFB3 (Obach *et al*., 2004; Cao *et al*., 2019), I assumed that the male-enriched expression of *Pfkfb3* would ensure male-predominant glycolytic activity. Accordingly, when knockdown was used to decrease the level of *Pfkfb3* gene expression in male-derived fibers to that observed in female-derived fibers, the glycolytic activity in the former decreased to levels similar to those observed in the latter. As previously noted, the male-predominant glycolytic activity of fast-twitch muscles is thought to be due to the greater number of type IIB fibers in male muscles. Furthermore, this study demonstrated for the first time that male type IIB fibers are intrinsically capable of driving glycolysis more vigorously than female fibers through the male-biased expression of a single gene, *Pfkfb3*.

Specifically, the results of this study suggest the relationship between the sexually dimorphic expression of *Pfkfb3* and its potential significance. To date, studies so far have investigated the mechanism of *Pfkfb3* gene regulation from the perspective of glycolysis promotion in cancer cells. These studies implicated HIF1α (hypoxia inducible factor 1α) in the regulation of gene expression (Obach *et al*., 2004; Mole *et al*., 2009). Moreover, testosterone and E2 have been found to activate *HIF1α* gene expression in prostate (Massie *et al.*, 2011; Ragnum *et al*., 2013) and breast cancer cells (Imbert-Fernandez *et al*., 2014), respectively, suggesting that sex steroids could induce *Pfkfb3* gene expression through *HIF1α* induction.

Meanwhile, the current study of the quadriceps muscle suggested that still-unidentified factors besides testosterone might be responsible for the male-enriched expression of *Pfkfb3*. There are two possible reasons why I assume it. The first reason lies in the complexed endocrine system in the testis, in which functionally different four hormones are secreted from two cell types; Leydig cells secrete testosterone and insulin peptide 3 (INSL3), and Sertoli cells secrete anti-Mullerian hormones (AMH) and inhibin B (InhB) (Chong *et al*, 2017). In this study, castrated male mice were subjected to DHT treatments (the active form of testosterone). Therefore, my results could not exclude the possibility that testicular factors other than testosterone affect the expression of *Pfkfb3*. Second, there is a possibility that genes localized on the sex chromosomes might be attributable to the male-enriched expression of *Pfkfb3* and eventually sexually dimorphic metabolisms seen in XX and XY muscle fibers. Among these factors, it is interesting to note that the metabolic activities of preimplantation embryos are higher in males than in females (Ray *et al*., 1995), and the number of X chromosomes may cause the sexually dimorphic metabolism (Chen *et al*., 2012). Because histone demethylase, UTX (KDM6A), UTY, SMCX (KDM5C), and SMCY (KDM5D) are encoded by the sex chromosomes, it is worth analyzing their contribution for regulation of cellular metabolisms by utilizing the gene knockout mice.

Female-predominant fatty acid β-oxidation due to E2-activated expression of Pdk4

Using type IIB fibers, the present study confirmed once again the well-known fact that females preferentially utilize fatty acids for mitochondrial oxidation. This preference has been suggested by E2-induced expression of genes involved in fatty acid β-oxidation, including *Cpt1b* (which encodes a rate-limiting enzyme for β-oxidation), carnitine palmitoyltransferase (Drynan *et al*., 1996; Houten *et al*., 2010), *Hadhb* (hydroxyacyl-CoA dehydrogenase), and *Pdk4* (pyruvate dehydrogenase kinase 4) (Campbell *et al*., 2003). The results using whole gastrocnemius muscles are in agreement with the present findings using type IIB fibers, in that the induction ratio of *Pdk4* by E2 was more apparent than those of other β-oxidation genes.

It has been demonstrated that PDK4 induces a metabolic shift from glycolysis to fatty acid β-oxidation through phosphorylation, thereby suppressing the pyruvate dehydrogenase complex (Wu *et al*., 1998). It has been shown that the level of *Pdk4* gene expression correlates with the activity of fatty acid β-oxidation in cultured cells (Pettersen *et al*., 2019). Taken together, I inferred that the preferential use of fatty acid β-oxidation in females is caused primarily by *Pdk4* gene expression induced by E2. As anticipated, E2 treatment enhanced fatty acid-dependent mitochondrial oxygen consumption in female-derived muscle fibers, and this enhancement was abolished by the knockdown of *Pdk4*. Although I cannot exclude the possibility that female-predominant fatty acid β-oxidation is attributable to E2-activated β-oxidation genes

such as *Cpt1b*, the knockdown studies of cultured muscle fibers indicated that E2-induced *Pdk4* gene expression was a more likely responsible.

Furthermore, we also observed E2-induced expression of the *Pcx* gene, whose product mediates an anaplerotic reaction to maintain tricarboxylic acid cycle flux by providing oxaloacetate. This reaction is critical for maintenance of the oxidative function in mitochondria in skeletal muscle (Davis Bremer, 1980; Gibala *et al*., 2000). Thus, *Pdk4* and *Pcx* may function to coordinate female-predominant mitochondrial fatty acid β-oxidation through simultaneous induction by E2.

Studies have demonstrated that cardiac muscle fibers of women have a higher activity of fatty acid β-oxidation than those of men (Kadkhodayan *et al*., 2017; Ventura-Clapier *et al*., 2017). This female-biased fatty acid β-oxidation was observed in the mice that developed a hypertrophied heart following exercise (Foryst-Ludwig *et al*., 2011). In order to understand the mechanism responsible for the sexually dimorphic metabolism, transcriptomes were obtained from the cardiac muscles of both sexes (Trexler *et al*., 2017; Camila *et* al., 2020; Synnergren *et al*., 2020). Several genes involved in fatty acid utilization were found as female-enriched genes. Unfortunately, however, none of the studies identified *Pdk4* as the female-enriched gene, suggesting that distinct mechanism for female-biased fatty acid β-oxidation might work between the cardiac muscle and the type IIB fibers of skeletal muscle. Alternatively, since the effect of estrus cycle was not considered in those studies, experiments to investigate the

effects of E2 might reveal an involvement of PDK4/*Pdk4* in female-biased fatty acid β-oxidation in the cardiac muscle.

To reveal the molecular mechanisms regarding the effect of E2 on *Pdk4* expression, further analysis is needed. Previous studies have shown that the expression of *Pdk4* was enhanced in skeletal muscle by E2 (Campbell *et al*., 2003; Ronkainen *et al*., 2010; Salehzadeh *et al*., 2011). However, it is unclear whether this enhanced expression by E2 is a direct action of its receptor, ERα or ERβ. A study by Gao *et* al. (2008) revealed in mouse liver that *Pdk4* is one of the target genes of E2-bound ERα. Further studies using skeletal muscle fibers from knockout mice of ERα or ERβ and studies using agonist and antagonist molecules of ERs could reveal the detailed molecular mechanism.

Male-enriched polyamine biosynthetic genes and female-enriched extracellular matrix genes

Gene ontology analysis of male-enriched genes showed polyamine biosynthesis as the top term (Table 6). Indeed, genes related to this process, *Odc1, Amd1*, *Amd2*, and *Smox*, were found to be higher in male. Polyamine biosynthesis in skeletal muscle depends on androgen possibly through binding to androgen receptor (AR) (Lee & Maclean, 2014). A study by Sakakibara *et al.* (2021) reported similar results. Studies using AR knockout mouse model showed decreased expression of polyamine biosynthesis genes (MacLean *et al*., 2008; Lee *et al*., 2011; Kanou *et al*., 2021;

Sakakibara *et al*., 2021). Together, these results are consistent with our results regarding the male-enriched expression of the polyamine biosynthesis genes.

Several collagen genes were found to be higher in female than male. Collagen is one of the components for extracellular matrix (ECM) in addition to glycoproteins, proteoglycans, and elastin. By forming a network of intracellular connective tissue (IMCT), collagen plays roles as the central and fibrous component of ECM. IMCT can be divided into three layers, endomysium, perimysium, and epimysium. ECM plays important role in the development, growth, muscle repair and transmission of contractile force (Csapo *et al*., 2020). Thus, it was suggested that females have great protection against muscle damage or membrane disruption as a result of intense training (Salimena *et al*., 2004; Heinemeier *et al*., 2007).

The ultrastructure of skeletal muscle demonstrates that muscle fibers are surrounded by endomysium, a connective tissue composed of type I and III collagen fibrils. The structure connects to a basement membrane that directly surrounds each muscle fiber and is composed mainly of type IV and VI collagen (Dueweke et al., 2016). In this endomysium, besides fibroblast, the fibro-adipogenic progenitors (FAPs) also resides. Thus, the upregulated expression of various collagen genes seen in the transcriptome data might be due to contamination of this connective tissue. Since I manually separated and isolated a single muscle fiber using forceps under a microscope, the possibility of contamination could not be excluded. When fibers were cultured for

metabolic studies, I used collagenase I to obtain the single fiber. Therefore, contamination of the cells might be largely decreased in the fiber culture.

Conclusion and future direction

In this study, I investigated sexually dimorphic energy metabolism in type IIB fibers of quadriceps muscle. It should be noted that skeletal muscles are originated from cranial mesoderm or somite (Yoshioka et al., 2021), suggesting that muscles derived from the different origins may show different properties. Indeed, it has been reported that cranial mesoderm-derived and somite-derived muscle stem cells show different ability for muscle regeneration in aged mice. Since quadriceps muscle is derived from somite, a study using cranial mesoderm-derived muscles such as masseter to investigate sexually dimorphic utilization of the fuels regulated by PFKFB3 and PDK4 might be interesting. In addition, to ask a question whether every type of muscle fiber has preferences in energy-producing pathways, studies using other types of fibers (Type IIX, IIA, and I) or the same fiber (type IIB) in slow-twitch muscle, such as soleus, might give us more profound insights into vital roles of PFKFB3 and PDK4 in the sexually dimorphic energy metabolism in skeletal muscles.

It has been accepted that gonadal sex is determined by the presence or the absence of the Y chromosome-linked sex-determining gene, *SRY*, in many mammalian species, including human and mouse. Since not only gonadal cells but all other cells have Y chromosome, the involvement of Y-linked genes in establishment of sex differences has been suggested. From this point of view, it might be worth studying the involvement of Y-linked genes to establish sexually dimorphic features such as energy metabolism. As

I mentioned in the discussion section, I am attempting to investigate whether a Y-linked histone demethylase, *Uty*, is involved in the sexual dimorphism in skeletal muscles by using *Uty* knockout mice. Since UTY has been reported to induce gene expression by erasing repressive histone modification (H3K27me3), comparison of epigenome landscapes between wild-type male, *Uty* knockout male, and wild-type female might give a deeper understanding of the mechanism underlying sexually dimorphic expressions of genes, including *Pfkfb3* and *Pdk4*.

In conclusion, using the type IIB fibers of the quadriceps muscle as a model system, I succeeded in unmasking the mechanisms to induce male-predominant glycolysis and female-predominant fatty acid oxidation. The sexually dimorphic metabolism was shown to be achieved possibly by two genes, namely *Pdk4* and *Pfkfb3*, through transcriptional regulation by estradiol and unknown factor(s), respectively. Considering that skeletal muscle is the largest energy-consuming organ in the human body, my present findings may contribute to understanding the mechanism underlying sexually different energy metabolisms. Specifically, these results may provide new insight into the metabolic properties of females, whose E2 concentrations vary throughout life and during the estrus cycle. In the present study, I evaluated the characteristics of a single type of muscle fiber type IIB.

REFERENCES

Aizawa, K. *et al.* Sex differences in steroidogenesis in skeletal muscle following a single bout of exercise in rats. *J. Appl. Physiol.* **104**, 67-74 doi:10.1152/japplphysiol.00558.2007 (2008).

Alderman, M. H. & Taylor, H. S. Molecular mechanisms of estrogen action in female genital tract development. *Differentiation*. **118**, 34-40 doi: 10.1016/j.diff.2021.01.002 (2021).

Almacellas, E. *et al.* Phosphofructokinases Axis Controls Glucose-Dependent mTORC1 Activation Driven by E2F1. *iScience*. **20**, 434-448 doi:10.1016/j.isci.2019.09.040 (2019).

Augusto, V., Padovani, C. R. & Campos, G. E. R. Skeletal Muscle Fiber Types in C57BL6J Mice. *Brazilian J. Morphol. Sci.* **21**, 89-94 (2004).

Axell, A. M. *et al.* Continuous testosterone administration prevents skeletal muscle atrophy and enhances resistance to fatigue in orchidectomized male mice. *Am. J. Physiol. - Endocrinol. Metab.* **291**, E506-E516 doi:10.1152/ajpendo.00058.2006 (2006).

Bachman, J. F. *et al*. Prepubertal skeletal muscle growth requires Pax7-expressing satellite cell-derived myonuclear contribution. *Development*. **145**, 1-13 doi:10.1242/dev.167197 (2018).

Ball-Burnett, M., Green, H. J., & Houston, M. E. Energy metabolism in human slow and fast twitch fibres during prolonged cycle exercise. *J. Physiol.* **437**, 257-267 doi:10.1113/jphysiol.1991.sp018594 (1991).

Behr, S. C., Courtier, J. L., & Qayyum, A. Imaging of mullerian duct anomalies. *Radiographics*. **32**, E233-250 doi:10.1148/rg.326125515 (2012).

Berchtold, M. W., Brinkmeier, H. & Müntener, M. Calcium ion in skeletal muscle: Its crucial role for muscle function, plasticity, and disease. *Physiol. Rev.* **80**, 1215-1265 doi:10.1152/physrev.2000.80.3.1215 (2000).

Bhasin, S. *et al*. The mechanisms of androgen effects on body composition: mesenchymal pluripotent cell as the target of androgen action. *J. Gerontol. A. Biol. Sci. Med. Sci.* **58**, M1103-10 doi:10.1093/gerona/58.12.m1103 (2003).

Bongers, K. S. *et al.* Spermine oxidase maintains basal skeletal muscle gene expression and fiber size and is strongly repressed by conditions that cause skeletal muscle atrophy. *Am. J. Physiol. - Endocrinol. Metab.* **308**, E144–E158 doi:10.1152/ajpendo.00472.2014 (2015).

Brouillette, J., Rivard, K., Lizotte, E., & Fiset, C. Sex and strain differences in adult mouse cardiac repolarization: importance of androgens. *Cardiovasc. Res*. **65**, 148-157 doi:10.1016/j.cardiores.2004.09.012 (2005).

Brown, M. Skeletal muscle and bone: effect of sex steroids and aging. *Adv. Physiol. Educ.* **32**, 120-126 doi:10.1152/advan.90111.2008 (2008).

Cabral, A. M., Vasquez, E. C., Moyses, M. R., & Antonio, A. Sex hormone modulation of ventricular hypertrophy in sinoaortic denervated rats. *Hypertension*. **11**, I93-97 doi: 10.1161/01.hyp.11.2_pt_2.i93 (1988).

Camila, M. *et al*. Sex differences in gene expression and regulatory networks across 29 human tissues. *Cell Rep*. **31**, 107795 doi:10.1016/j.celrep.2020.107795 (2020).

Campbell, S. E., Mehan, K. A., Tunstall, R. J., Febbraio, M. A. & Cameron-Smith, D. 17β-Estradiol upregulates the expression of peroxisome proliferator-activated receptor α and lipid oxidative genes in skeletal muscle. *J. Mol. Endocrinol.* **31**, 37-45 doi:10.1677/jme.0.0310037 (2003).

Cao, Y. *et al.* PFKFB3-mediated endothelial glycolysis promotes pulmonary hypertension. *Proc. Natl. Acad. Sci. U. S. A.* **116**, 13394-13403 doi:10.1073/pnas.1821401116 (2019).

Cervelli, M. *et al.* Skeletal Muscle Pathophysiology: The Emerging Role of Spermine Oxidase and Spermidine. *Med. Sci.* **6**, 1-15 (2018) doi:10.3390/medsci6010014.

Chen, X. *et al.* The number of X chromosomes causes sex differences in adiposity in mice. *PLoS Genet.* **8**, e1002709 doi:10.1371/journal.pgen.1002709 (2012).

Chidi-Ogbulu, N. & Baar, K. Effect of estrogen on musculoskeletal performance and injury risk. *Front. Physiol.* **9**, 1-11 doi:10.3389/fphys.2018.01834 (2019)

Chong, Y. H., Pankhurst, M. W., & Mclennan, I. S. The testicular hormones AMH, InhB, INSL3, and testosterone can be independently deficient in older men. *J. Gerontol. A. Biol. Sci. Med. Sci.* **72**, 548-553 doi:10.1093/gerona/glw143 (2017).

Colliander, E. B., Dudley, G. A., & Tesch, P. A. Skeletal muscle fiber type composition and performance during repeated bouts of maximal, concentric contractions. *Eur. J. Appl. Physiol Occup. Physiol.* **58**, 81-86 doi:10.1007/BF00636607 (1988).

Corciulo, C. *et al*. Pulsed administration for physiological estrogen replacement in mice. *F1000Res.* **10**, 1-19 doi:10.12688/f1000research.54501.1 (2021).

Csapo, R., Gumpenberger, M., & Wessner, B. Skeletal muscle extracellular matrix - what do we know about its composition, regulation, and physiological roles? A narrative review. *Front. Physiol.* **11**, 1-15 doi:10.3389/fphys.2020.00253 (2020).

Davis, E. J., Spydevold & Bremer, J. Pyruvate Carboxylase and Propionyl-CoA Carboxylase as Anaplerotic Enzymes in Skeletal Muscle Mitochondria. *Eur. J. Biochem.* **110**, 255-262 doi:10.1111/j.1432-1033.1980.tb04863.x (1980).

DeNardi, C. *et al.* Type 2X-myosin heavy chain is coded by a muscle fiber type-specific and developmentally regulated gene. *J. Cell Biol.* **113**, 823-835 doi:10.1083/jcb.123.4.823 (1993).

Devries, M. C. Sex-based differences in endurance exercise muscle metabolism: Impact on exercise and nutritional strategies to optimize health and performance in women. *Exp. Physiol.* **101**, 243-249 doi:10.1113/EP085369 (2016).

Dobin, A. *et al.* STAR: Ultrafast universal RNA-seq aligner. *Bioinformatics*. **29**, 15-21 doi:10.1093/bioinformatics/bts635 (2013).

Drynan, L., Quant, P. A. & Zammit, V. A. Flux control exerted by mitochondrial outer membrane carnitine palmitoyltransferase over β-oxidation, ketogenesis and tricarboxylic acid cycle activity in hepatocytes isolated from rats in different metabolic states. *Biochem. J.* **317**, 791-795 doi:10.1042/bj3170791 (1996).

Dubois, V., Laurent, M., Boonen, S., Vanderschueren, D., & Claessens, F. Androgens and skeletal muscle: cellular and molecular action mechanisms underlying the anabolic actions. *Cell. Mol. Life. Sci.* **69**, 1651-1667 doi:10.1007/s00018-011-0883-3 (2012).

Dueweke, J. J., Awan, T. M., & Mendias, C. L. Regeneration of Skeletal Muscle After Eccentric Injury. *J. Sport Rehabil.* **26**, 171-179 doi: 10.1123/jsr.2016-0107 (2016).

Eason, J.M., Schwartz, G. A., Pavlath, G. K., & English, A. W. Sexually dimorphic expression of myosin heavy chains in the adult mouse masseter. *J. Appl. Physiol.* **89**, 251-258 doi:10.1152/jappl.2000.89.1.251 (2000).

Eisenberg, T. *et al.* Induction of autophagy by spermidine promotes longevity. *Nat. Cell Biol.* **11**, 1305-1314 doi:10.1038/ncb1975 (2009).

Enns, D. L. & Tiidus, P. M. The influence of estrogen on skeletal muscle: sex matters. *Sports Med.* **40**, 41-58 doi:10.2165/11319760-000000000-00000 (2010).

Erben, R. G. *et al*. Deletion of deoxyribonucleic acid binding domain of the vitamin D receptor abrogates genomic and nongenomic functions of vitamin D. *Mol. Endocrinol.* **16**, 1524-1537 doi:10.1210/mend.16.7.0866 (2002).

Fitts, J. M., Klein, R. M., & Powers, C. A. Comparison of tamoxifen and testosterone propionate in male rats: differential prevention of orchidectomy effects on sex organs, bone mass, growth, and the growth hormone-IGF-I axis. *J. Androl.* **25**, 523-534 doi:10.1002/j.1939-4640.2004.tb02823.x (2004).

Foryst-Ludwig, A. *et al*. Sex differences in physiological cardiac hypertrophy are associated with exercise-mediated changes in energy substrate availability. *Am J Physiol. Heart. Circ. Physiol.* **301**, 115-122 doi:10.1152/ajpheart.01222.2010 (2011).

Frontera, W. R., & Ochala, J. Skeletal muscle, a brief review of structure and function. *Calcif. Tissue Int*. **96**, 183-195 doi:10.1007/s00223-014-9915-y (2015).

Gallot, Y. S., Hindi, S. M., Mann, A. K. & Kumar, A. Isolation, culture, and staining of single myofibers. *Bio-protocol.* **6**, e1942 doi:10.21769/BioProtoc.1942 (2016).

Gao, H., Falt, S., Sandelin, A., Gustafsson, J-A., & Dahlman-Wright, K. Genome-wide identification of estrogen receptor α-binding sites in mouse liver. *Mol. Endocrinol.* **22**, 10-22 doi:10.1210/me.2007-0121 (2008).

Garcia-Cazarin, M. L., Snider, N. N., & Andrande, F. H. Mitochondrial isolation from skeletal muscle. *J. Vis. Exp*. 49, e2452 doi:10.3791/2452 (2011).

Ghobadi, N., Sahraei, H., Meftahi., G. H., Bananej, M., & Salehi, S. Effect of estradiol replacement in ovariectomized NMRI mice in response to acute and chronic stress. *J. App. Pharm. Sci.* **6**, 176-184 doi:10.7324/JAPS.2016.601128 (2016).

Gibala, M. J., Young, M. E. & Taegtmeyer, H. Anaplerosis of the citric acid cycle: Role in energy metabolism of heart and skeletal muscle. in *Acta Physiol. Scand.* **168**, 657-665 doi:10.1046/j.1365-201X.2000.00717.x (2000).

Glenmark, B. *et al.* Difference in skeletal muscle function in males vs. females: Role of estrogen receptor-β. *Am. J. Physiol. - Endocrinol. Metab.* **287**, 1125–1131 doi:10.1152/ajpendo.00098.2004 (2004).

Goodman, C. A., Kotecki, J. A., Jacobs, B. L. & Hornberger, T. A. Muscle fiber type-dependent differences in the regulation of protein synthesis. *PLoS One*. **7**, e37890 doi:10.1371/journal.pone.0037890 (2012).

Gorza, L. Identification of a novel type 2 fiber population in mammalian skeletal muscle by combined use of histochemical myosin ATPase and anti-myosin monoclonal antibodies. *J. Histochem. Cytochem.* **38**, 257-265 doi:10.1177/38.2.2137154 (1990).

Green, H. J., Fraser, I. G. & Ranney, D. A. Male and female differences in enzyme activities of energy metabolism in vastus lateralis muscle. *J. Neurol. Sci.* **65**, 323-331 doi:10.1016/0022-510X(84)90095-9 (1984).

Haizlip, K. M., Harrison, B. C. & Leinwand, L. A. Sex-based differences in skeletal muscle kinetics and fiber-type composition. *Physiology.* **30**, 30-39 doi:10.1152/physiol.00024.2014 (2015).

Hamalainen, N. & Pette, D. The histochemical profiles of fast fiber types IIB, IID, and IIA in skeletal muscles of mouse, rat, and rabbit. *J. Histochem. Cytochem.* **41**, 733-743 doi:10.1177/41.5.8468455 (1993).

Haren, M. T. *et al.* Testosterone modulates gene expression pathways regulating nutrient accumulation, glucose metabolism and protein turnover in mouse skeletal muscle. *Int. J. Androl.* **34**, 55-68 doi:10.1111/j.1365-2605.2010.01061.x (2011).

Hargreaves, M. & Spriet, L. L. Skeletal muscle energy metabolism during exercise. *Nat. Metab.* **2**, 817-828 doi:10.1038/s42255-020-0251-4 (2020).

Hassan, MA. M., Lavery, S. A., & Trew, G. H. Congenital uterine anomalies and their impact on fertility. *Womens Health (Lond).* **6**, 443-461 doi:10.2217/whe.10.19 (2010).

Heinemeier, K. M. *et al*. Expression of collagen and related growth factors in rat tendon and skeletal muscle in response to specific contraction types. *J. Physiol.* **582**, 1303-1316 doi:10.1113/jphysiol.2007.127639 (2007).

Herbison, G. J., Jaweed, M. M. & Ditunno, J. F. Muscle fiber types. *Arch. Phys. Med. Rehabil.* **63**, 227-230 (1982).

Horton, R. & Tait, J. F. In vivo conversion of dehydroisoandrosterone to plasma androstenedione and testosterone in man. *J. Clin. Endocrinol. Metab.* **27**, 79-88 doi:10.1210/jcem-27-1-7 (1967).

Houten, S. M. & Wanders, R. J. A. A general introduction to the biochemistry of mitochondrial fatty acid β-oxidation. *J. Inherit. Metab. Dis.* **33**, 469-477 doi:10.1007/s10545-010-9061-2 (2010).

Hulmi, J. J. *et al*. Androgen receptors and testosterone in men--effects of protein ingestion, resistance exercise and fiber type. *J. Steroid Biochem. Mol. Biol.* **110**, 130-137 doi:10.1016/j.jsbmb.2008.03.030 (2008).

Hunter, S. K. The relevance of sex differences in performance fatigability. *Med. Sci. Sports Exerc.* **48**, 2247-2256 doi:10.1249/MSS.0000000000000928 (2016).

Hüttner, S. S. *et al.* Isolation and culture of individual myofibers and their adjacent muscle stem cells from aged and adult skeletal muscle. in *Methods Mol. Biol.* **2045**, 25-36 doi:10.1007/7651_2019_209 (2019).

Idris, A. I. Ovariectomy/orchidectomy in rodents. *Methods Mol. Biol.* **816**, 545-551 doi:10.1007/978-1-61779-415-5_34 (2012).

Igarashi, K. & Kashiwagi, K. Modulation of cellular function by polyamines. *IUBMB Life*. **67**, 160-169 doi: 10.1002/iub.1363 (2015).

Imbert-Fernandez, Y. *et al.* Estradiol stimulates glucose metabolism via 6-phosphofructo-2-kinase (PFKFB3). *J. Biol. Chem.* **289**, 9440-9448 doi:10.1074/jbc.M113.529990 (2014).

Jacobs, I., Tesch, P. A., Bar-Or, O., Karlsson, J. & Dotan, R. Lactate in human skeletal muscle after 10 and 30 s of supramaximal exercise. *J. Appl. Physiol. Respir. Environ. Exerc. Physiol.* **55**, 365-367 doi:10.1152/jappl.1983.55.2.365 (1983).

Julien, I. B., Sephton, C. F., & Dutchak, P. A. Metabolic networks influencing skeletal muscle fiber composition. *Front. Cell Dev. Biol.* **6**, 1-6 doi:10.3389/fcell.2018.00125 (2018)

Kadkhodayan, A. *et al*. Sex affects myocardial blood flow and fatty acid substrate metabolism in humans with nonischemic heart failure. *J. Nucl. Cardiol*. 24, 1226-1235 doi:10.1007/s12350-016-0467-6 (2017).

Kanou, M. *et al.* Polyamine pathway is associated with muscle anabolic effects by androgen receptor ligand. *JCSM Rapid Communications*. **4**, 57-74 doi:10.1002/rco2.28 (2021).

Kim, J. H. *et al*. Sex hormones establish a reserve pool of adult muscle stem cells. *Nat. Cell Biol*. **18**, 930-940 doi:10.1038/ncb3401 (2016).

Kitajima, S. *et al.* Undifferentiated State Induced by Rb-p53 Double Inactivation in Mouse Thyroid Neuroendocrine Cells and Embryonic Fibroblasts. *Stem Cells*. **33**, 1657-1669 doi:10.1002/stem.1971 (2015).

Kitajima, Y., Ogawa, S. & Ono, Y. Visualizing the functional heterogeneity of muscle stem cells. in *Methods Mol Biol.* **1516**, 183-193 doi:10.1007/7651_2016_349 (2016).

Kohn, F. M. Testosterone and body functions. *Aging Male.* **9**, 183-188 doi:10.1080/13685530601060396 (2006).

Kumar, A., Accorsi, A., Rhee, Y., & Girgenrath, M. Do's and don'ts in the preparation of muscle cryosections for histological analysis. *J. Vis. Exp.* **99**, e52793 doi:10.3791/52793 (2015).

Laredo, S. A. *et al*. Nongenomic effects of estradiol on aggression under short day photoperiods. *Horm*. *Behav*. **64**, 557-565 doi:10.1016/j.yhbeh.2013.06.002 (2013).

Lee, N. K. & Maclean, H. Polyamines, androgens, and skeletal muscle hypertrophy. *J. Cell. Physiol*. **226**, 1453-1460 doi:10.1002/jcp.22569 (2011).

Lee, N. K. L., Skinner, J. P. J., Zajac, J. D., & MacLean, H. E. Ornithine decarboxylase is upregulated by the androgen receptor in skeletal muscle and regulates myoblast proliferation. *Am. J. Physiol. Endocrinol. Metab.* **301**, E172-179 doi:10.1152/ajpendo.00094.2011 (2011).

Lin, I. H. *et al.* Skeletal muscle in aged mice reveals extensive transformation of muscle gene expression. *BMC Genet.* **19**, 1-13 doi:10.1186/s12863-018-0660-5 (2018).

Liu, J., liang, XJ., & Gan, ZJ. Transcriptional regulatory circuits controlling muscle fiber type switching. *Sci. China Life Sci*. **58**, 321-327 doi:10.1007/s11427-015-4833-4 (2015).

Lundsgaard, A-M. & Kiens, B. Gender differences in skeletal muscle substrate metabolism - molecular mechanisms and insulin sensitivity. *Front. Endocrinol (Lausanne).* **13**, 1-16 doi:10.3389/fendo.2014.00195 (2014).

MacLean, H. E. *et al*. Impaired skeletal muscle development and function in male, but not female, genomic androgen receptor knockout mice. *FASEB J.* **22**, 2676-2689 doi:10.1096/fj.08-105726 (2008).

Madeo, F., Eisenberg, T., Pietrocola, F. & Kroemer, G. Spermidine in health and disease. *Science*. **359**, eaan2788 doi:10.1126/science.aan2788 (2018).

Maher, A. C., Akhtar, M., Vockley, J. & Tarnopolsky, M. A. Women have higher protein content of β-oxidation enzymes in skeletal muscle than men. *PLoS One*. **5**, e12025 doi:10.1371/journal.pone.0012025 (2010).

Mahlapuu, M. *et al.* Expression profiling of the □-subunit isoforms of AMP-activated protein kinase suggests a major role for □3 in white skeletal muscle. *Am J Physiol Endocrinol Metab.* **286**, E194-200 doi: 10.1152/ajpendo.00147.2003 (2004).

Marin, P., Krotkiewski, M., & Bjorntorp, P. Androgen treatment of middle-aged, obese men: effects on metabolism, muscle and adipose tissues. *Eur. J. Med.* **1**, 329-336 (1992).

Massie, C. E. *et al.* The androgen receptor fuels prostate cancer by regulating central metabolism and biosynthesis. *EMBO J.* **30**, 2719-2733 doi:10.1038/emboj.2011.158 (2011).

Melouane, A., Ghanemi, A., Aubé, S., Yoshioka, M. & St-Amand, J. Differential gene expression analysis in ageing muscle and drug discovery perspectives. *Ageing Res. Rev.* **41**, 53-63 doi:10.1016/j.arr.2017.10.006 (2018).

Mole, D. R. *et al.* Genome-wide association of hypoxia-inducible factor (HIF)-1α and HIF-2α DNA binding with expression profiling of hypoxia-inducible transcripts. *J. Biol. Chem.* **284**, 16767-16775 doi:10.1074/jbc.M901790200 (2009).

Morton, R. W. *et al*. Muscle androgen receptor content but not systemic hormones is associated with resistance training-induced skeletal muscle hypertrophy in healthy, young men. *Front. Physiol.* **9**, 1-11 doi:10.3389/fphys.2018.01373 (2018).

Mulukutla, B. C., Yongky, A., Daoutidis, P. & Hu, W. S. Bistability in glycolysis pathway as a physiological switch in energy metabolism. *PLoS One* **9**, e98756 doi:10.1371/journal.pone.0098756 (2014).

Murach, K. *et al.* Single muscle fiber gene expression with run taper. *PLoS One* **9**, e108547 doi:10.1371/journal.pone.0108547 (2014).

Nelson, J. F., Felicio, L. S., Randall, P. K., Sims, C. & Finch, C. E. A longitudinal study of estrous cyclicity in aging C57BL/6J mice: I. Cycle frequency, length and vaginal cytology. *Biol. Reprod.* **27**, 327-339 doi:10.1095/biolreprod27.2.327 (1982).

Nishimura, K. *et al.* Essential role of S-adenosylmethionine decarboxylase in mouse embryonic development. *Genes Cells*. **7**, 41-47 doi:10.1046/j.1356-9597.2001.00494.x (2002).

O'Connell, M. D. L., & Wu, F. C. W. Androgen effects on skeletal muscle: implications for the development and management of frailty. *Asian J. Androl.* **16**, 203-212 doi:10.4103/1008-682X.122581 (2014).

Obach, M. *et al.* 6-Phosphofructo-2-kinase (pfkfb3) gene promoter contains hypoxia-inducible factor-1 binding sites necessary for transactivation in response to hypoxia. *J. Biol. Chem.* **279**, 53562-53570 doi:10.1074/jbc.M406096200 (2004).

Ophoff, J. *et al.* Androgen signaling in myocytes contributes to the maintenance of muscle mass and fiber type regulation but not to muscle strength or fatigue. *Endocrinology*. **150**, 3558-3566 doi:10.1210/en.2008-1509 (2009).

Padilla-Banks, E., Jefferson, W. N., & Newbold, R. R. The immature mouse is a suitable model for detection of estrogenicity in the uterotropic bioassay. *Environ. Health Perspect.* **109**, 821-826 doi:10.1289/ehp.01109821 (2001).

Pasut, A., Jones, A. E. & Rudnicki, M. A. Isolation and culture of individual myofibers and their satellite cells from adult skeletal muscle. *J Vis Exp.* **73**, e50074 doi:10.3791/50074 (2013).

Pendeville, H. *et al.* The Ornithine Decarboxylase Gene Is Essential for Cell Survival during Early Murine Development. *Mol. Cell. Biol.* **21**, 6549-6558 doi:10.1128/mcb.21.19.6549-6558.2001 (2001).

Pette, D. & Staront, R. S. Mammalian skeletal muscle fiber type transitions. *Int. Rev. Cytol.* **170**, 143-223 doi:10.1016/s0074-7696(08)61622-8 (1997).

Pette, D. Metabolic heterogeneity of muscle fibres. *J. Exp. Biol.* **115**, 179-189 doi:10.1242/jeb.115.1.179 (1985).

Pettersen, I. K. N. *et al.* Upregulated PDK4 expression is a sensitive marker of increased fatty acid oxidation. *Mitochondrion.* **49**, 97-110 doi:10.1016/j.mito.2019.07.009 (2019).

Pillon, N. J. *et al.* Transcriptomic profiling of skeletal muscle adaptations to exercise and inactivity. *Nat. Commun.* **11**, 1-15 doi:10.1038/s41467-019-13869-w (2020).

Quarmby, V. E., Fox-Davies, C., & Korach, K. S. Estrogen action in the mouse uterus: the influence of the neuroendocrine-adrenal axis. *Endocrinology*. **114**, 108-115 doi:10.1210/endo-114-1-108 (1984).

Quiroga, H. P. O., Goto, K., & Zammit, P. S. Isolation, cryosection and immunostaining of skeletal muscle. *Methods Mol. Biol.* **1460**, 85-100 doi:10.1007/978-1-4939-3810-0_8 (2016).

Ragnum, H. B. *et al.* Hypoxia-independent downregulation of hypoxia-inducible factor 1 targets by androgen deprivation therapy in prostate cancer. *Int. J. Radiat. Oncol. Biol. Phys.* **87**, 753-760 doi:10.1016/j.ijrobp.2013.07.023 (2013).

Rana, K. *et al.* Muscle-specific androgen receptor deletion shows limited actions in myoblasts but not in myofibers in different muscles in vivo. *J. Mol. Endocrinol.* **57**, 125-138 doi:10.1530/JME-15-0320 (2016).

Rana, K., Lee, N. K. L., Zajac, J. D. & Maclean, H. E. Expression of androgen receptor target genes in skeletal muscle. *Asian J. Androl.* **16**, 675-683 doi:10.4103/1008-682X.122861 (2014).

Raudrant, D. & Rabe, T. Progestogens with antiandrogenic properties. *Drugs*. **63**, 463-492 doi:10.2165/00003495-200363050-00003 (2003).

Ray, P. F., Conaghan, J., Winston, R. M. L. & Handyside, A. H. Increased number of cells and metabolic activity in male human preimplantation embryos following in vitro fertilization. *J. Reprod. Fertil.* **104**, 165-171 doi:10.1530/jrf.0.1040165 (1995).

Robbins, J. B., Broadwell, C., Chow, L. C., Parry, J. P., & Sadowski, E. A. Müllerian duct anomalies: embryological development, classification, and MRI assessment. *J. Magn. Reson. Imaging.* **41**, 1-12 doi: 10.1002/jmri.24771 (2015)

Ronkainen, P. H. A. *et al*. Global gene expression profiles in skeletal muscle of monozygotic female twins discordant for hormone replacement therapy. *Aging cell.* **9**, 1098-1110 doi:10.1111/j.1474-9726.2010.00636.x (2010).

Rosa-Caldwell, M. E. & Greene, N. P. Muscle metabolism and atrophy: Let's talk about sex. *Biol. Sex Differ.* **10**, 1–14 doi:10.1186/s13293-019-0257-3 (2019).

Rovira, J., Irimia, J. M., Guerrero, M., Cadefau, J. A. & Cussó, R. Upregulation of heart PFK-2/FBPase-2 isozyme in skeletal muscle after persistent contraction. *Pflugers Arch. Eur. J. Physiol.* **463**, 603-613 doi:10.1007/s00424-011-1068-5 (2012).

Safari, T., Nematbakhsh, M., Evans, R. G., & Denton, K. M. High-dose estradiol replacement therapy enhances the renal vascular response to angiotensin II via an AT2-receptor dependent mechanism. *Adv. Pharmacol. Sci.* **2015**, 1-7 doi:10.1155/2015/682745 (2015).

Sakakibara, I. *et al*. Myofiber androgen receptor increases muscle strength mediated by a skeletal muscle splicing variant of Mylk4. *iScience*. **24**, 102303 doi:10.1016/j.isci.2021.102303 (2021).

Salehzadeh, F., Rune, A., Osler, M., & Al-Khalili, L. Testosterone or 17(beta)-estradiol exposure reveals sex-specific effects on glucose and lipid metabolism in human myotubes. *J. Endocrinol.* **210**, 219-229 doi:10.1530/JOE-10-0497 (2011).

Salimena, M. C., Lagrota-Candido, J., & Quirico-Santos, T. Gender dimorphism influences extracellular matrix expression and regeneration of muscular tissue in mdx dystrophic mice. *Histochem Cell Biol.* **122**, 435-444 doi:10.1007/s00418-004-0707-8 (2004).

Sawano, S. *et al.* A one-step immunostaining method to visualize rodent muscle fiber type within a single specimen. *PLoS One.* **11**, e0166080 doi:10.1371/journal.pone.0166080 (2016).

Schiaffino, S. & Reggiani, C. Fiber types in Mammalian skeletal muscles. *Physiol. Rev.* **91**, 1447-1531 doi:10.1152/physrev.00031.2010 (2011).

Schiaffino, S. *et al.* Three myosin heavy chain isoforms in type 2 skeletal muscle fibres. *J. Muscle Res. Cell Motil.* **10**, 197-205 doi:10.1007/BF01739810 (1989).

Schindelin, J. *et al.* Fiji: An open-source platform for biological-image analysis. *Nat. Methods*. **9**, 676-682 doi:10.1038/nmeth.2019 (2012).

Scott, W., Stevens, J., & Binder-Macleod, S. A. Human skeletal muscle fiber type classifications. *Phys. Ther.* **81**, 1810-1816 doi:10.1093/ptj/81.11.1810 (2001).

Shima, H., Tsuji, M., Young P., & Cunha, G. R. Postnatal growth of mouse seminal vesicle is dependent on 5 alpha-dihydrotestosterone. *Endocrinology*. **127**, 3222-3233 doi:10.1210/endo-127-6-3222 (1990).

Sinha-Hikim, I. *et al*. Testosterone-induced increase in muscle size in healthy young men is associated with muscle fiber hypertrophy. *Am. J. Physiol. Endrocinol. Metab.* **283**, e154-164 doi:10.1152/ajpendo.00502.2001 (2002).

Sinha-Hikim, I., Cornford, M., Gaytan, H., Lee, M. L. & Bhasin, S. Effects of testosterone supplementation on skeletal muscle fiber hypertrophy and satellite cells in community-dwelling older men. *J. Clin. Endocrinol. Metab.* **91**, 3024–3033 doi:10.1210/jc.2006-0357 (2006).

Sipila, S. *et al*. Sex hormones and skeletal muscle weakness. *Biogerontology*. **14**, 231-245 doi: 10.1007/s10522-013-9425-8 (2013).

Synnergren, J. *et al*. Transcriptional sex and regional differences in paired human atrial and ventricular cardiac biopsies collected in vivo. *Physiol. Genomics*. **52**, 110-120 doi:10.1152/physiolgenomics.00036 (2020).

Tian, J. C. *et al*. Effect of androgen deprivation on the expression of aquaporins in rat prostate and seminal vesicle. *Andrologia*. **48**, 268-276 doi:10.1111/and.12442 (2015).

Trexler, C. L., Odell, A. T., Jeong, M. Y., Dowell, R. D., & Leinwand, L. A. Transcriptome and functional profile of cardiac myocytes is influenced by

biological sex. *Circ. Cardiovasc. Genet*. **10**, e001770 doi:10.1161/circgenetics.117.001770 (2017).

Uchitomi, R., *et al*. Metabolomic analysis of skeletal muscle in aged mice. *Sci. Rep.* **9**, 10425 doi:10.1038/s41598-019-46929-8 (2019).

Urban, R. J. *et al*. Testosterone administration to elderly men increases skeletal muscle strength and protein synthesis. *Am. J. Physiol.* **269**, E820-826 doi:10.1152/ajpendo.1995.269.5.E820 (1995).

Valkenburg, K. C., Amend, S. R., & Pienta, K. J. Murine prostate micro-dissection and surgical castration. *J. Vis. Exp.* **111, e**53984 doi:10.3791/53984 (2016).

Van Schaftingen, E., Hue, L. & Hers, H. G. Fructose 2,6-bisphosphate, the probable structure of the glucose- and glucagon-sensitive stimulator of phosphofructokinase. *Biochem. J.* **192**, 897-901 doi:10.1042/bj1920897 (1980).

Ventura-Clapier, R. *et al*. Sex in basic research: concepts in the cardiovascular field. *Cardiovasc. Res*. **113**, 711-724 doi:10.1093/cvr/cvx066 (2017).

Wakley, A. A., Wiley, J. L. & Craft, R. M. Gonadal hormones do not alter the development of antinociceptive tolerance to delta-9-tetrahydrocannabinol in adult rats. *Pharmacol. Biochem. Behav.* **133**, 111-121 doi:10.1016/j.pbb.2015.03.021 (2016).

Wang, M., Yu, H., Kim, Y. S., Bidwell, C. A. & Kuang, S. Myostatin facilitates slow and inhibits fast myosin heavy chain expression during myogenic differentiation. *Biochem. Biophys. Res. Commun.* **426**, 83-88 doi:10.1016/j.bbrc.2012.08.040 (2012).

Weiss, A. *et al.* Organization of human and mouse skeletal myosin heavy chain gene clusters is highly conserved. *Proc. Natl. Acad. Sci. U. S. A.* **96**, 2958-2963 doi:10.1073/pnas.96.6.2958 (1999).

Welle, S., Tawil, R. & Thornton, C. A. Sex-related differences in gene expression in human skeletal muscle. *PLoS One.* **3**, e1385 doi:10.1371/journal.pone.0001385 (2008).

Westerblad, H., Bruton, J. D., & Katz, A. Skeletal muscle: energy metabolism, fiber types, fatigue and adaptibility. *Exp. Cell Res*. **316**, 3093-3099 doi:10.1016/j.yexcr.2010.05.019 (2010).

Wierman, M. E. Sex steroid effect at target tissues: mechanisms of action. *Adv. Physiol. Educ.* **31**, 26-33 doi:10.1152/advan.00086.2006 (2007).

Wu, C., Khan, S. A., Peng, L. J. & Lange, A. J. Roles for fructose-2,6-bisphosphate in the control of fuel metabolism: Beyond its allosteric effects on glycolytic and gluconeogenic enzymes. *Adv. Enzyme Regul.* **46**, 72-88 doi:10.1016/j.advenzreg.2006.01.010 (2006).

Wu, P. *et al.* Starvation and diabetes increase the amount of pyruvate dehydrogenase kinase isoenzyme 4 in rat heart. *Biochem. J.* **329**, 197-201 doi:10.1042/bj3290197 (1998).

Wüst, R. C. I., Morse, C. I., De Haan, A., Jones, D. A. & Degens, H. Sex differences in contractile properties and fatigue resistance of human skeletal muscle. *Exp. Physiol.* **93**, 843-850 doi:10.1113/expphysiol.2007.041764 (2008).

Yalcin, A., Telang, S., Clem, B. & Chesney, J. Regulation of glucose metabolism by 6-phosphofructo-2-kinase/fructose-2,6-bisphosphatases in cancer. *Exp. Mol. Pathol.* **86**, 174-179 doi:10.1016/j.yexmp.2009.01.003 (2009).

Yang, L., Smyth Gordon K & Wei, S. featureCounts: an efficient general purpose program for assigning sequence reads to genomic features. *Bioinformatics.* **30**, 923-930 doi: 10.1093/bioinformatics/btt656 (2014).

Yoshioka, M., Boivin, A., Bolduc, C. & St-Amand, J. Gender difference of androgen actions on skeletal muscle transcriptone. *J. Mol. Endocrinol.* **39**, 119–133 doi:10.1677/JME-07-0027 (2007).

Yoshioka, M., Boivin, A., Ye, P., Labrie, F. & St-Amand, J. Effects of dihydrotestosterone on skeletal muscle transcriptome in mice measured by serial analysis of gene expression. *J. Mol. Endocrinol.* **36**, 247-259 doi:10.1677/jme.1.01964 (2006).

Zierath, J. R. & Hawley, J. A. Skeletal muscle fiber type: influence on contractile and metabolic properties. *PLoS Biol.* **2,** e348 doi: 10.1371/journal.pbio.0020348 (2004).

Zitzmann, M. & Nieschlag, E. Testosterone levels in healthy men and the relation to behavioural and physical characteristics: facts and constructs. *Eur. J. Endocrinol.* **144**, 183-197 doi:10.1530/eje.0.1440183 (2001).

ACKNOWLEDGEMENTS

I would like to express my sincere gratitude to my supervisor Prof. Ken-Ichirou Morohashi for his continuous support, patience, motivation, enthusiasm, and immense knowledge throughout my study. Also, I wish to express my gratitude to Associate Prof. Takashi Baba for helpful discussion and technical advice. I would like to thank Dr. Yuuki Imai and Dr. Hiroshi Sakai (Medical School, Ehime University) and Dr. Hirotoshi Tanaka and Dr. Hiroki Yamazaki (The Institute of Medical Science, The University of Tokyo) for their technical advice and discussion, Dr. Yusuke Ono (Institute of Molecular Embryology and Genetics, Kumamoto University) for technical support of skeletal muscle culture, Dr. Akihito Harada and Dr. Yasuyuki Ohkawa (Division of Transcriptomics, Medical Institute of Bioregulation, Kyushu University) for providing anti-MYH2B and anti-MYH2A antibodies, and Dr. Mikita Suyama (Division of Bioinformatics, Medical Institute of Bioregulation, Kyushu University) for computational analyses of the sequence datasets. I also thank the Research Support Center, Research Center for Human Disease Modeling, Kyushu University Graduate School of Medical Sciences for technical assistance. Finally, I thank all the current and past members of Morohashi laboratory for their support and discussion. I would also like to express my gratitude to Ministry of Finance of the Republic of Indonesia, Secretariat General Indonesia Endowment Fund for Education (LPDP), for the doctoral scholarship.

LIST OF FIGURES

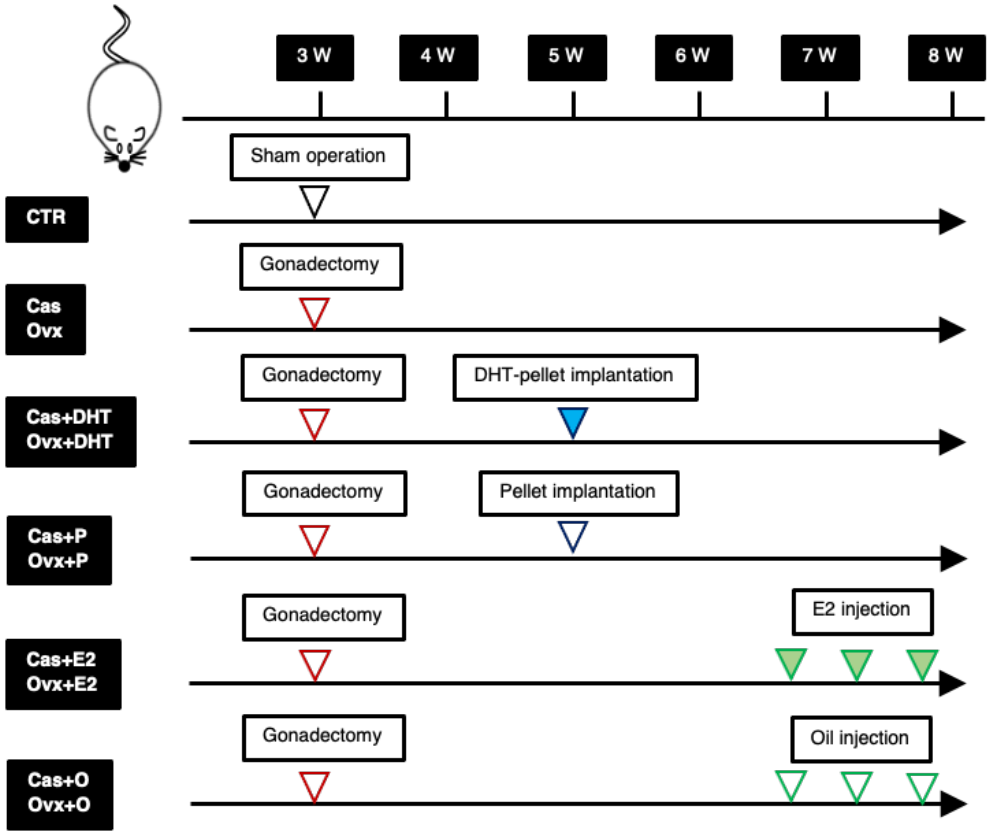

Figure 1. ***Timetable for operation and sex steroid treatments.***

Three weeks after birth, mice were gonadectomized (castration (Cas) and ovariectomy (Ovx)), or sham-operated (control (CTR)). The gonadectomized mice were implanted with DHT-pellet (Cas+DHT and Ovx+DHT) at 5-week, or E2-dissolved oil was injected three times at 47-day, 51-day, and 55-day (Cas+E2 and Ovx+E2). For the controls of the DHT and E2 treatments, an empty pellet was implanted (Cas+P and Ovx+P) and oil was injected (Cas+O and Ovx+O). Skeletal muscles were isolated from these mice at 8-week. Skeletal muscles of 8 experimental groups (male CTR, female CTR, Cas, Ovx, Cas+DHT, Ovx+DHT, Cas+E2, and OVX+E2) were used for the study of CSA size measurement, whereas 10 experimental groups (male CTR, female CTR, Cas+DHT, Ovx+DHT, Cas+P, Ovx+P, Cas+E2, OVX+E2, Cas+O, and Ovx+O) were used for transcriptome studies.

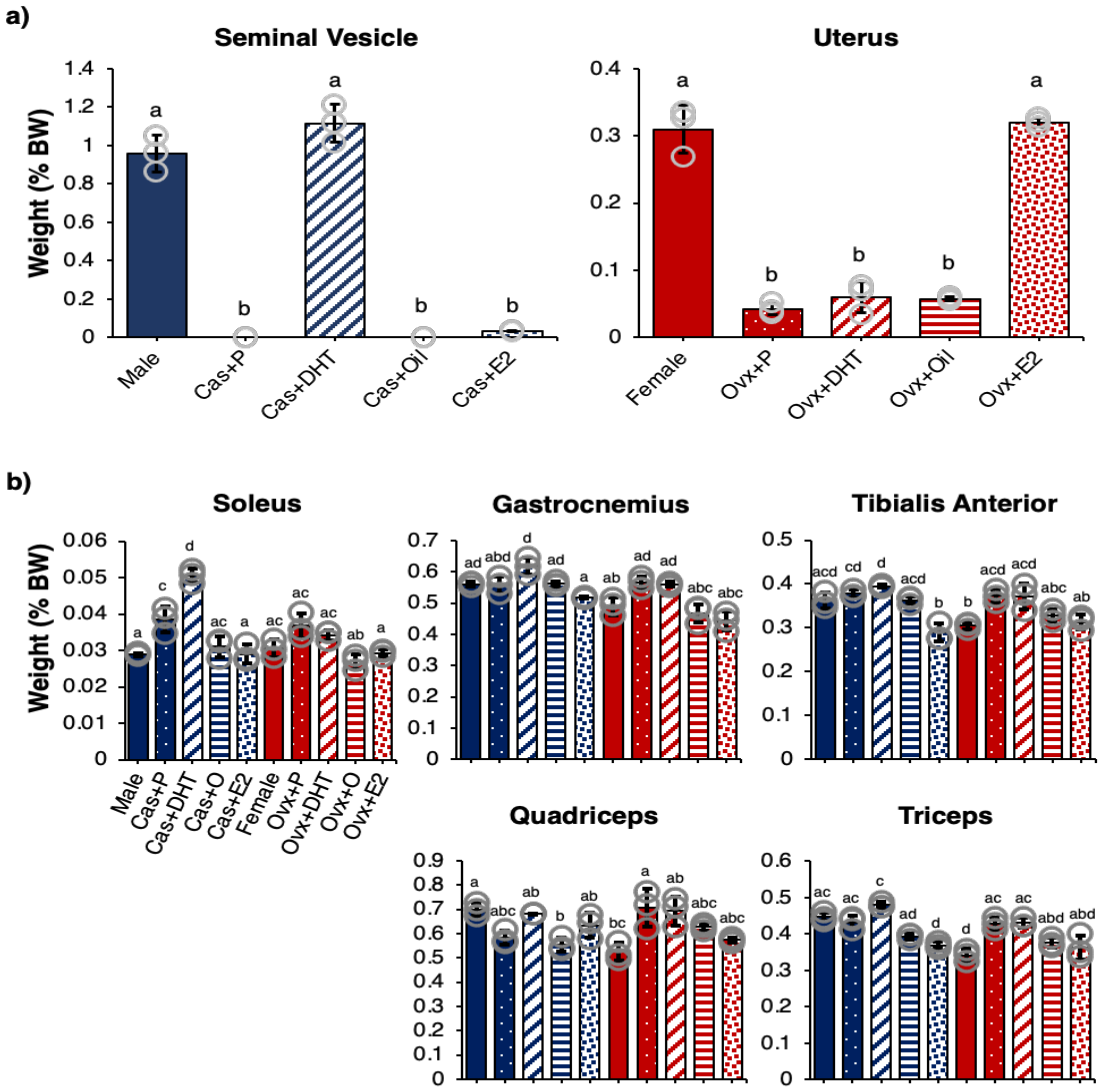

Figure 2. ***Weights of sex accessory organs and skeletal muscles after treatments.***

The sex accessory organs (uterus for female, seminal vesicle for male) and five skeletal muscles (soleus, gastrocnemius, tibialis anterior, quadriceps and triceps) were isolated from 8 weeks old mice in 10 experimental groups and weighted. **a)** Ratios of the weights of seminal vesicle (left) and uterus (right) to body weights are shown. **b)** Ratio of the weights between the five skeletal muscles and body weight are shown. Three biologically independent samples were analyzed. The data are presented as means ± SD. **p<0.01 with the same letter are not significantly different from each other (p<0.01).

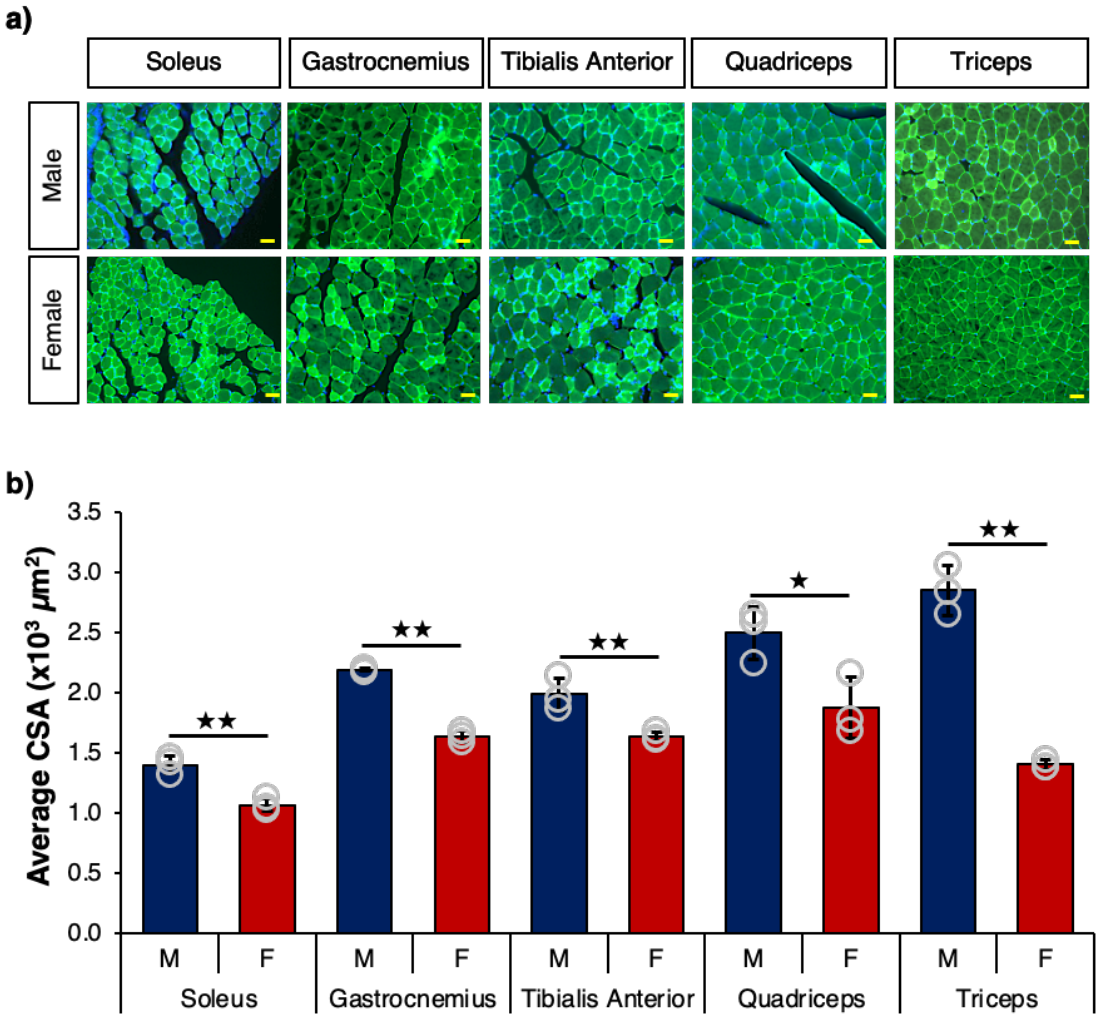

Figure 3. ***Sexually different skeletal muscle CSAs.***

a) Skeletal muscles fibers indicated were subjected to immunofluorescence study with antibodies against laminin (green). DAPI (blue) was used to stain the nuclei. Eight-week-old male and female mice were used. Bars = 50 μm. **b)** Cross-sectional areas (CSAs) were determined by calculating fiber size from three different random areas of muscles (around 100 fibers each random area). The tibialis anterior, gastrocnemius, quadriceps, triceps, and soleus muscles of 8-week-old male (M) and female (F) mice were used. Three biologically independent muscle samples were used. The data are shown as means ± SD. **p<0.01.

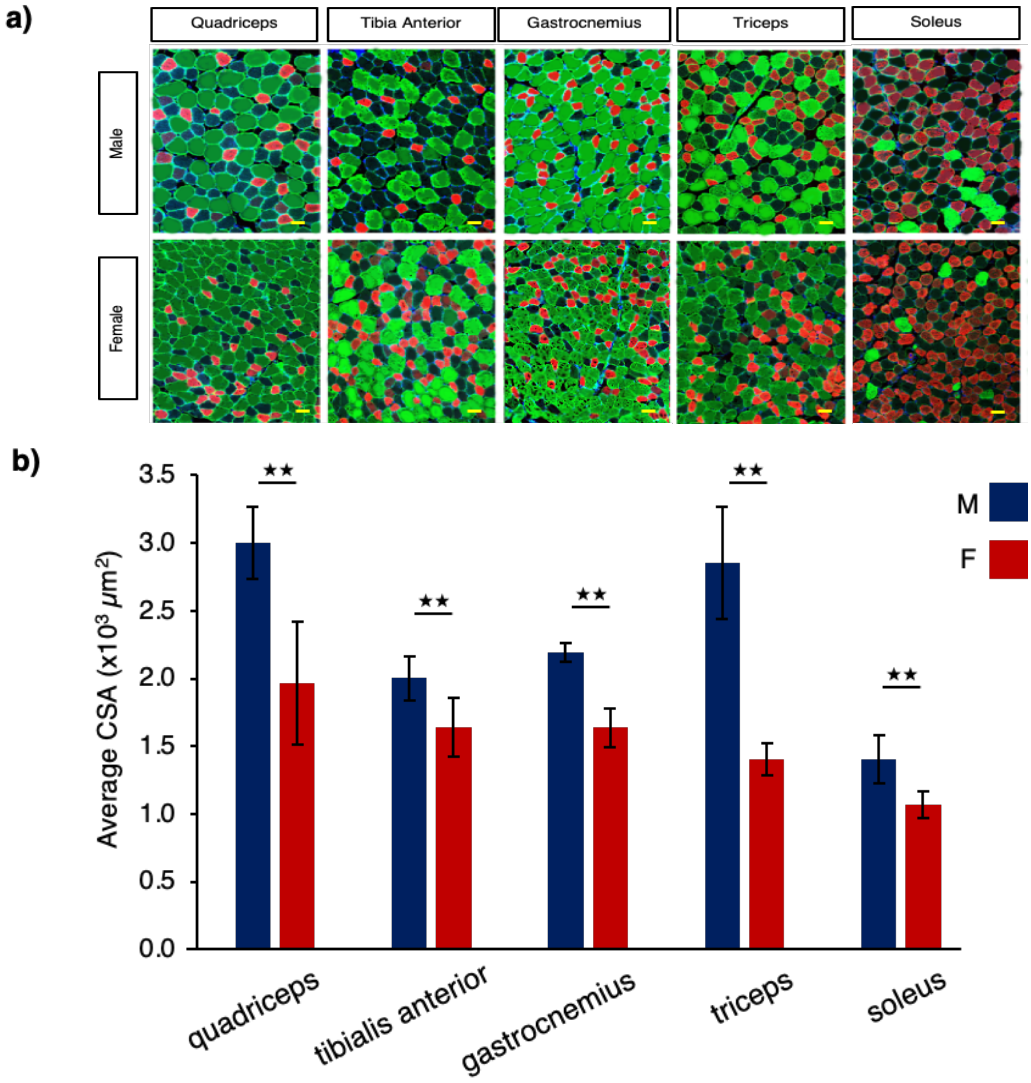

Figure 4. ***Sexually different CSA of type IIB muscle fibers.***

a) Type IIA (red) and type IIB (green) fibers of the skeletal muscles indicated at the figure were immunostained with antibodies against MYH2A and MYH2B, respectively. Eight-week-old male and female mice were used. Bars = 50 μm. **b)** Cross-sectional areas (CSAs) were determined using approximately 3000, 6000, 6000, 4000, and 50 fibers from the tibialis anterior, gastrocnemius, quadriceps, triceps, and soleus muscles of 8-week-old male (M) and female (F) mice, respectively. Three biologically independent muscle samples were used. The data are shown as means ± SD. **p<0.01.

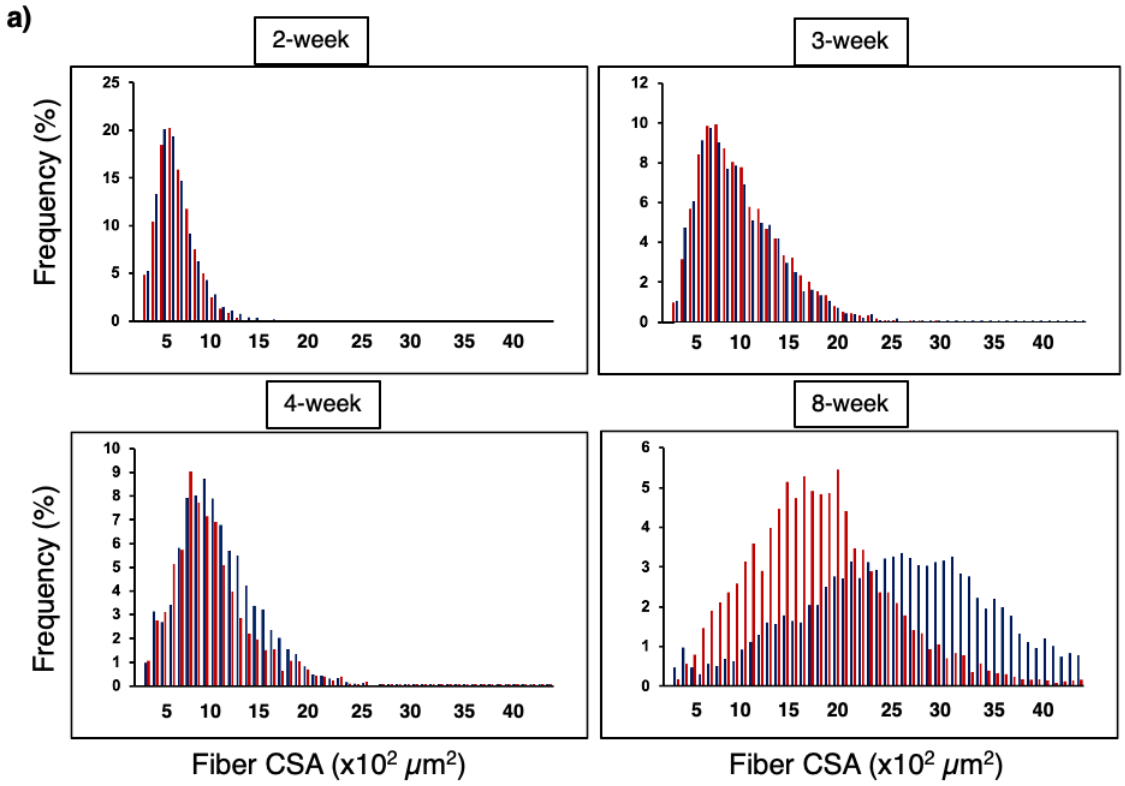
a)
2-week
3-week
4-week
8-week
Frequency (%)
Frequency (%)
Fiber CSA (x10² μm²)
Fiber CSA (x10² μm²)

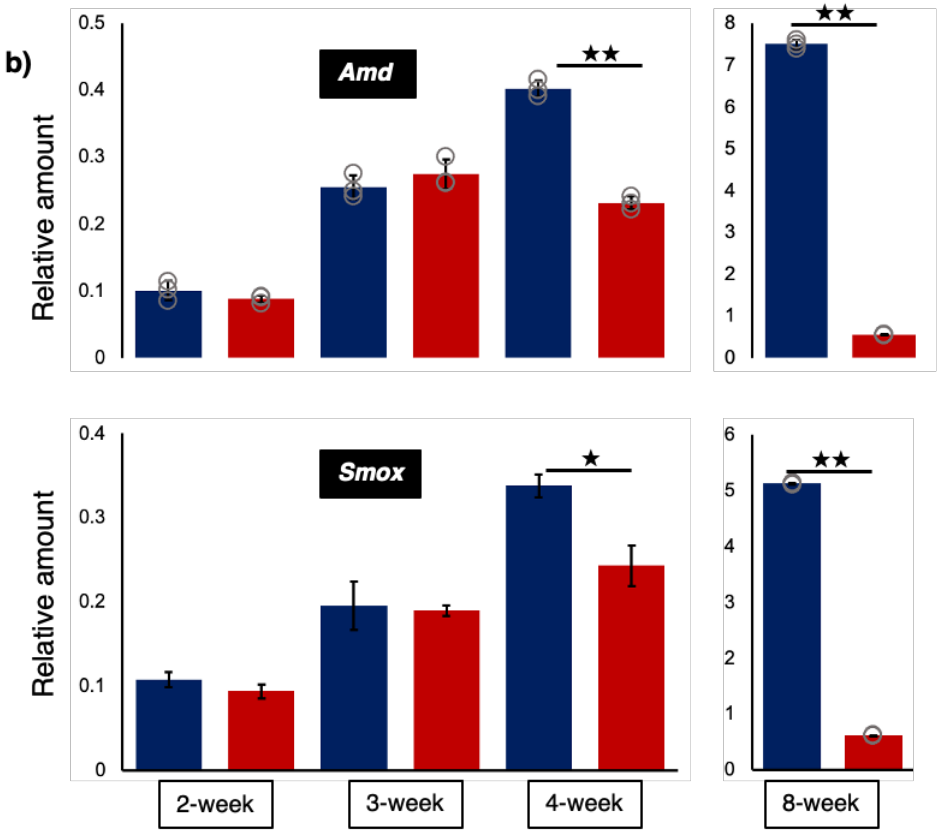
b)
Amd
Smox
Relative amount
Relative amount
★★
★
★★
2-week
3-week
4-week
8-week

Figure 5. ***Postnatally appeared sexually dimorphic features of skeletal muscle fibers.*** **a)** CSAs of type IIB fibers in quadriceps muscles were determined at 2, 3, 4 and 8 weeks after birth. The CSAs of more than 5000 fibers were determined for every three biologically independent samples. The distribution of the CSAs from male (M) and female (F) mice are indicated. Vertical and horizontal axes indicate the frequencies (%) of type IIB muscle fibers and their CSAs, respectively. **b)** Total RNAs were prepared from quadriceps type IIB fibers of male (M) and female (F) mice at 2, 3, 4, and 8 weeks after birth, then subjected to qRT-PCR for Amd and Smox genes. Three biologically independent samples were used. The data were normalized by *Actb* and are shown as means ± SD. The expression levels of the genes at 8 weeks are higher than those at earlier time points (compare vertical units of the graphs). *$p<0.05$, **$p<0.01$.
Blue bar = Male; Red bar = Female.

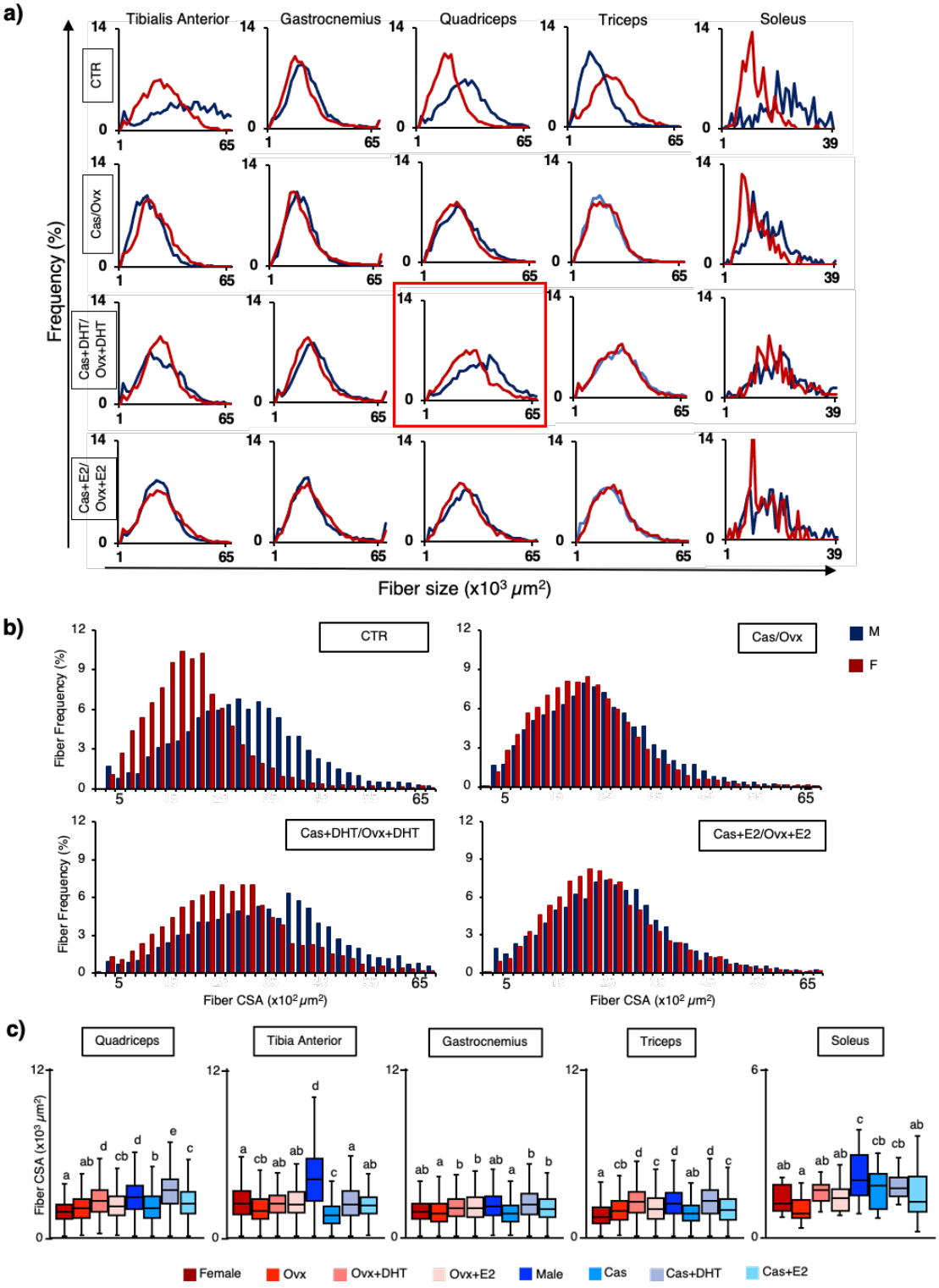
a)
Tibialis Anterior
Gastrocnemius
Quadriceps
Triceps
Soleus
CTR
Cas/Ovx
Cas+DHT/ Ovx+DHT
Cas+E2/ Ovx+E2
Frequency (%)
Fiber size (x10³ μm²)
b)
CTR
Cas/Ovx
Cas+DHT/Ovx+DHT
Cas+E2/Ovx+E2
M
F
Fiber Frequency (%)
Fiber CSA (x10² μm²)
c)
Quadriceps
Tibia Anterior
Gastrocnemius
Triceps
Soleus
Fiber CSA (x10³ μm²)
Female
Ovx
Ovx+DHT
Ovx+E2
Male
Cas
Cas+DHT
Cas+E2

Figure 6. ***Sexually dimorphic CSAs of type IIB fibers.***

a) CSAs of type IIB fibers in the tibialis anterior, gastrocnemius, quadriceps, triceps, and soleus muscles of sham-operated mice (CTR), gonadectomized mice (Cas, Ovx), DHT-treated mice after gonadectomy (Cas+DHT, Ovx+DHT), and E2-treated mice after gonadectomy (Cas+E2, Ovx+E2) were determined with three biologically independent samples. Representative CSA distributions of the muscles are shown. The average number of the fibers analyzed in CTR males, CTR females, Cas males, Ovx females, Cas+DHT males, Ovx+DHT females, Cas+E2 males, and Ovx+E2 females for the tibialis anterior were 2500, 2300, 3600, 3100, 4000, 3200, 3300, and 3300 fibers, respectively. Those for the gastrocnemius were 5900, 4600, 5700, 5400, 6200, 5100, 6700, and 4100 fibers, respectively. Those for the quadriceps were 5500, 4800, 4900, 5700, 4900, 5900, 6200, and 5900 fibers, respectively. Those for the triceps, 4500, 4300, 4800, 4200, 5200, 4200, 4800, and 4300 fibers, respectively. Those for the soleus, 50, 55, 65, 40, 65, 50, 63, 40 fibers, respectively. Male and female data are indicated by blue and red bars. Vertical and horizontal axes indicate frequencies (%) and fiber sizes, respectively. **b)** CSAs of type IIB fibers in the quadriceps was showed a sexual dimorphism in DHT-treated after gonadectomy. **c)** The CSA size distribution was compared among the eight experimental groups above. The data were analyzed as described in the Methods. The box and whisker plots with different letters denote significant differences between muscles ($p<0.01$).

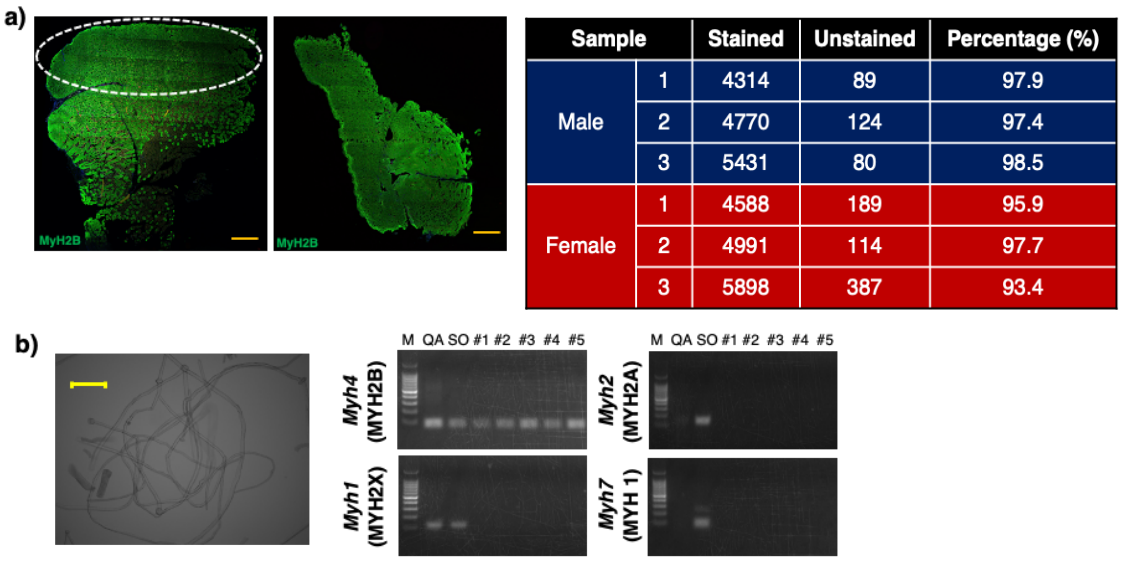

Sample		Stained	Unstained	Percentage (%)
Male	1	4314	89	97.9
	2	4770	124	97.4
	3	5431	80	98.5
Female	1	4588	189	95.9
	2	4991	114	97.7
	3	5898	387	93.4

Figure 7**.** ***Preparation of type IIB fibers for mRNA sequencing***

a) Preparation of the type IIB-enriched region in the quadriceps**.** The quadriceps muscle roughly consists of two regions with different colors, white (external region) and pale-reddish (internal region). These predominantly contain fast- and slow-type fibers, respectively. Immunofluorescence of a cross-section of the quadriceps muscle shows that most muscle fibers in the external region (enclosed by a white broken line) stain positively for MYH2B (green; left). By contrast, a substantial number of fibers in the internal region are unstained. The internal region was removed from the quadriceps muscle and a cross-section of the remaining external region underwent staining for further analysis (right). Scale bar = 500 μm. The numbers of fibers with and without MYH2B staining in the processed external region were counted in both male and female mice. Three biologically independent samples were analyzed in both sexes. **b)** Determination of fiber types prepared from the quadriceps**.** Two individual fibers prepared from the quadriceps muscle are shown on the left. Scale bar = 200 μm. The fiber type was determined by RT-PCR using RNAs prepared from individual fibers. RNAs prepared from whole quadriceps and soleus muscles were used as controls. *MYH4* (*myosin heavy chain 4*) encoding MYH2B, *MYH1* (*myosin heavy chain 1*) encoding MYH2X, *MYH2* (*myosin heavy chain 2*) encoding MYH2A, and *MYH7*

(*myosin heavy chain 7*) encoding MYH1 were used as the marker genes for type IIB, type IIX, type IIA, and type I fibers, respectively. When whole quadriceps (QA) and soleus (SO) muscles were used, the expressions of all of these *Myh* genes were detected. Only the expression of *Myh4* was detected in most of the individual fibers prepared (#1 - #5). RT-PCR images for the five fibers are shown. M = size marker.

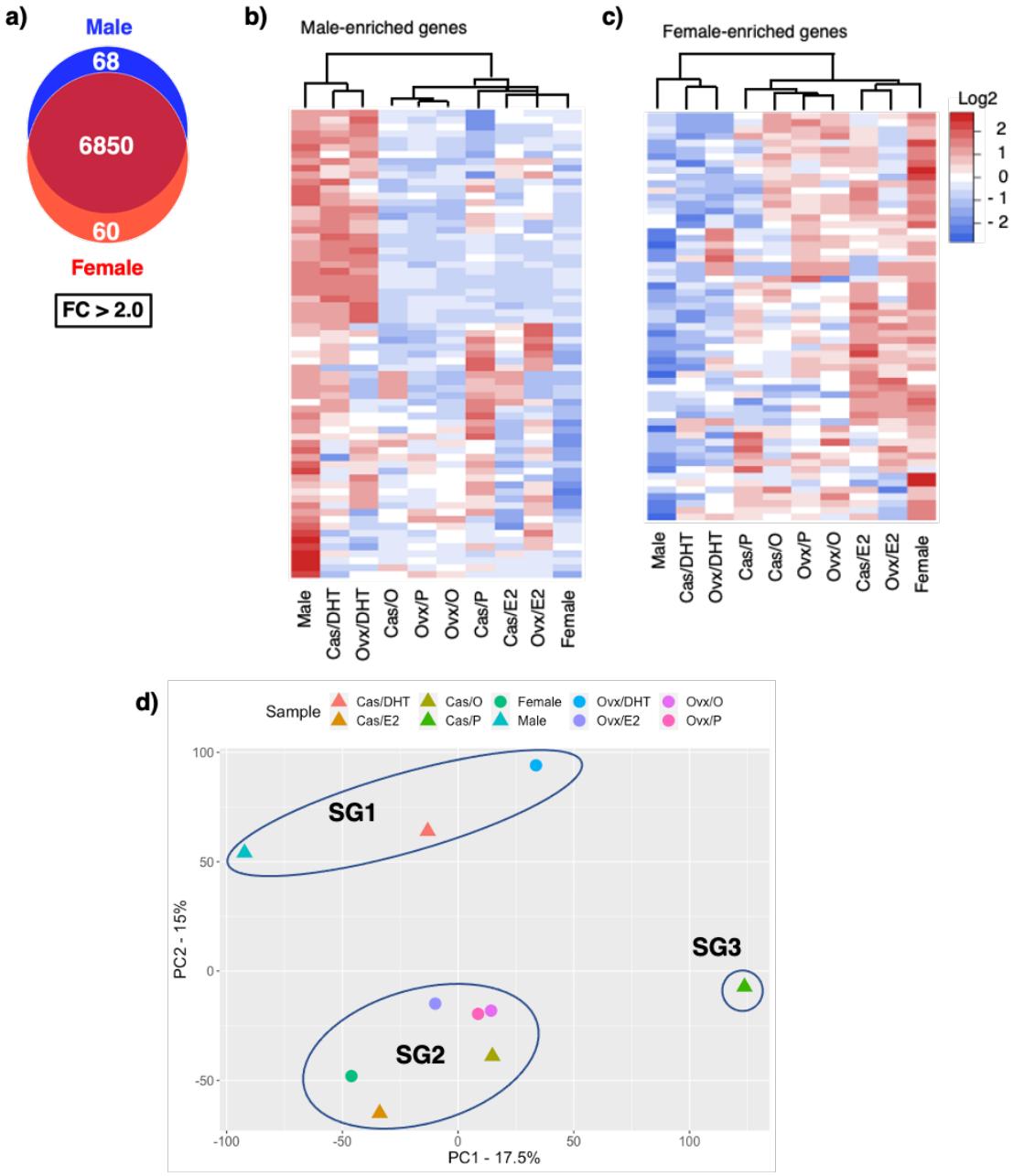

Figure 8. ***Sexually dimorphic gene expression in quadriceps type IIB fibers.***

a) A total of 6,978 genes whose CPM values were more than 10.0 in either of the two sexes (sham-operated males or females) were identified. Overall, 68 and 60 genes were revealed to be male enriched (M) and female enriched (F) by more than 2.0-fold, respectively. **b, c)** Heatmaps of the male-enriched and female-enriched gene expressions in the 10 experimental mouse groups (see text and Figure 1) are shown.

Color gradients is related to the z-score as indicated at the right. **d)** Results of principal component analysis of whole gene expression in the 10 groups are presented. PC1 and PC2 account for 17.5% and 15% of the percentage contribution to the variance, respectively. As indicated by closed ovals, the 10 groups are divided into three subgroups (SG1 to SG3).

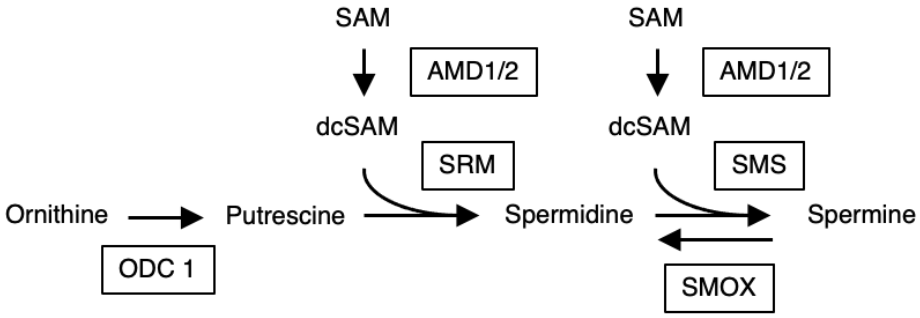

Gene	Male	Cas+P	Cas+DHT	Cas+O	Cas+E2	Female	Ovx+P	Ovx+DHT	Ovx+O	Ovx+E2
Odc1	137.3	46.1	155.7	43.1	36.1	47.0	46.7	103.3	35.7	35.2
Amd1/2	1561.7	153.5	1923.6	191.1	179.9	200.2	203.7	1596.0	169.5	146.4
Srm	4.8	8.5	4.3	6.0	6.4	3.4	5.0	5.6	4.5	4.2
Sms	110.1	79.0	99.1	84.2	80.6	110.7	85.6	93.1	85.2	75.9
Smox	468.6	58.7	363.0	117.7	90.6	106.5	105.1	533.6	123.6	80.1

Figure 9. ***Male-biased and androgen-dependent expression of the genes involved in polyamine synthetic pathway.***

(a) Polyamine synthetic pathway is shown with metabolites and enzymes (open boxes). SAM; S-adenosylmethionine, dcSAM; decarboxylated S-adenosylmethionine, AMD1/2; S-adenosylmethionine decarboxylase, ODC 1; Ornithine decarboxylase, SRM; Spermidine synthase, SMS; Spermine synthase, SMOX; spermine oxidase. ***(b)*** The expression of the polyamine synthetic genes in the 10 experimental groups is shown.

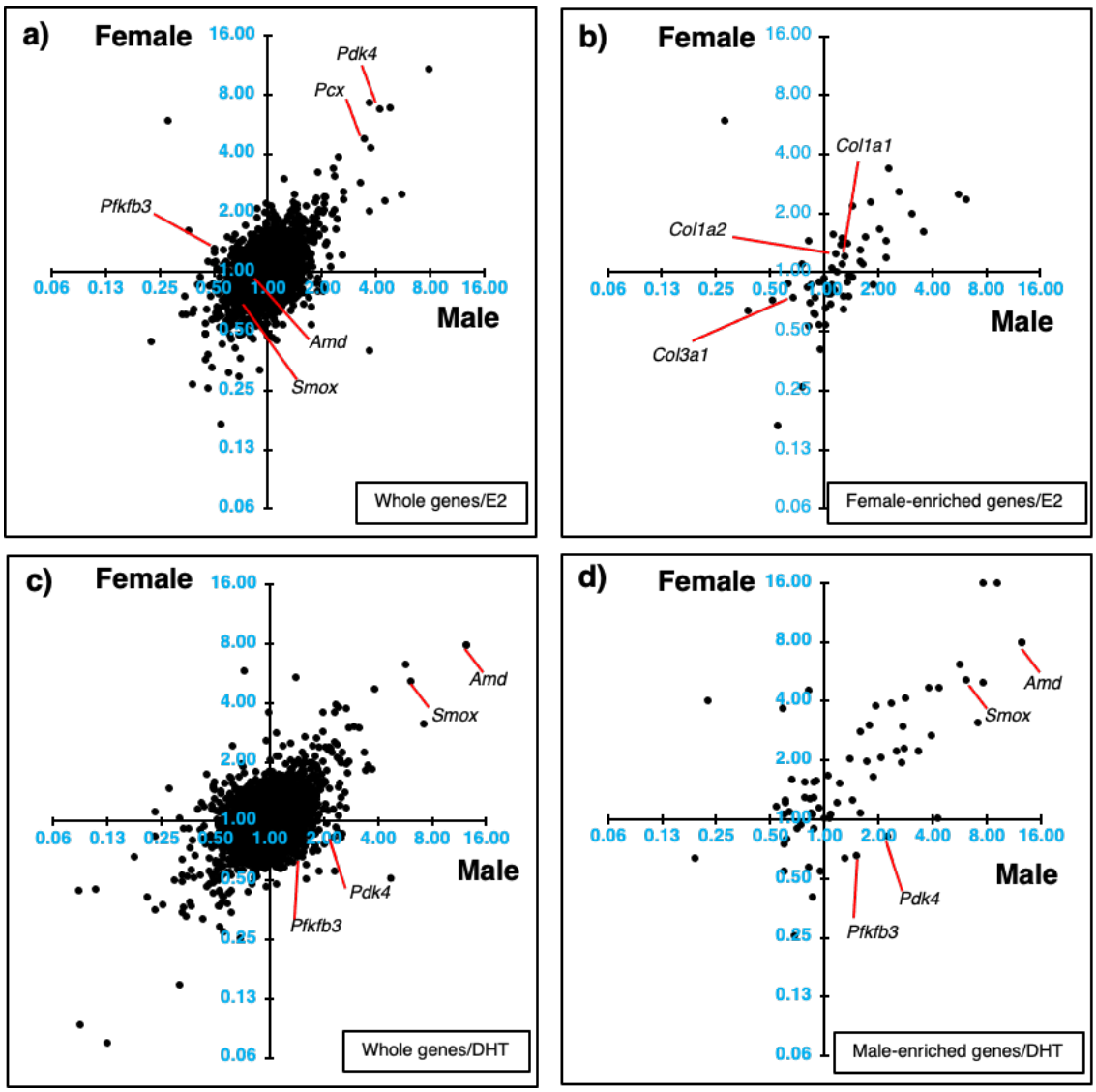

Figure 10. ***Identification of genes whose expression is potentially affected by sex steroids.***

a, b) Induction ratios by E2 treatment, namely, Cas+E2/Cas+O (horizontal axis) for males and Ovx+E2/Ovx+O (vertical axis) for females, were examined and plotted for all expressed genes **(a)** and for the female-enriched genes **(b)**. **c, d)** Induction ratios by DHT treatment, namely, Cas+DHT/Cas+P for males (horizontal axis) and Ovx+DHT/Ovx+P for females (vertical axis), were plotted for all expressed genes **(c)** and for the male-enriched genes **(d)**. The scales are logarithmic. The locations of *Pdk4*, *Pfkfb3*, *Pcx*, *Amd*, *Smox*, *Col1a1*, *Col1a2*, and *Col3a1*, are shown.

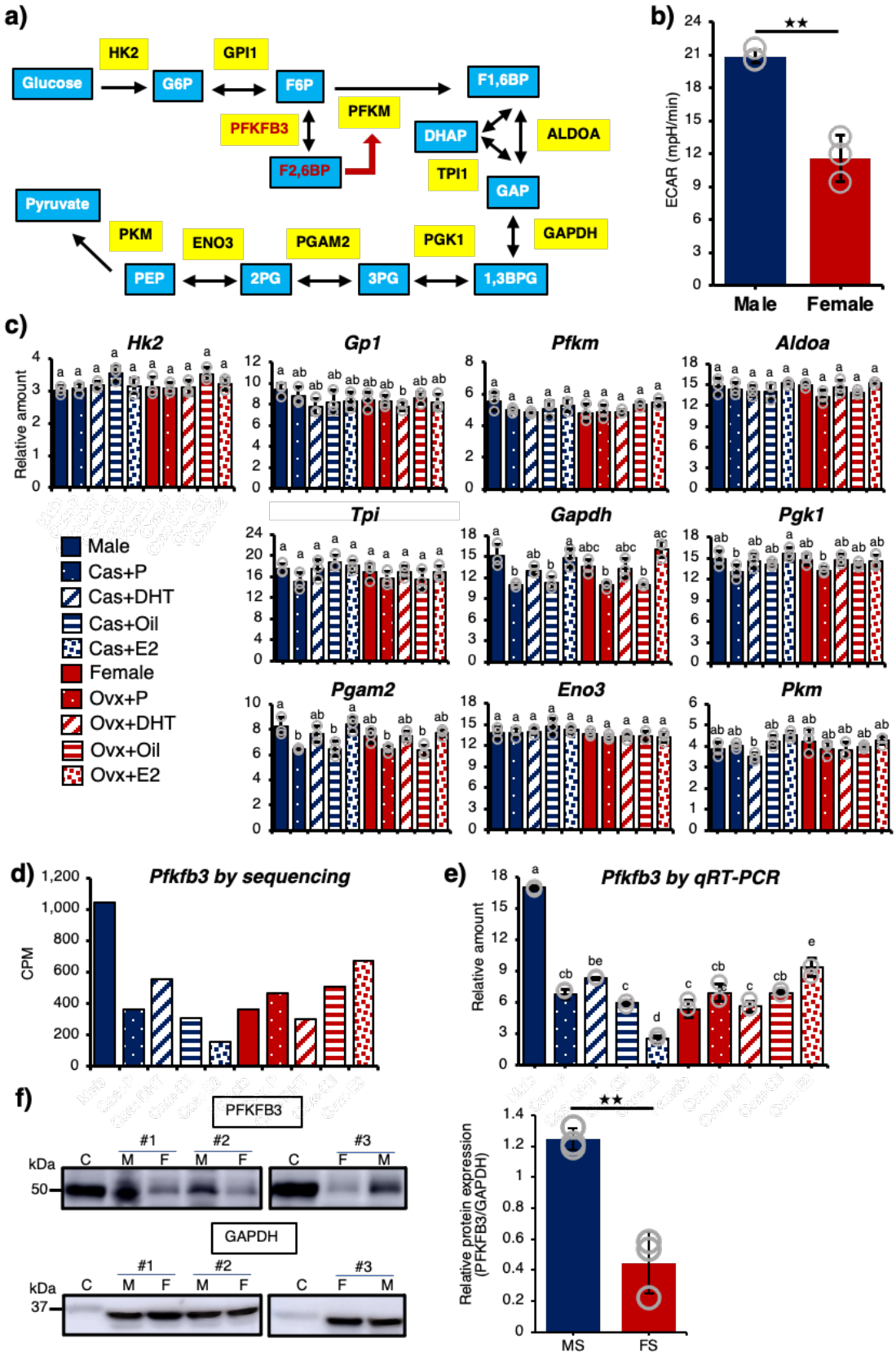
a)
Glucose
HK2
G6P
GPI1
F6P
PFKFB3
PFKM
F1,6BP
F2,6BP
DHAP
ALDOA
TPI1
GAP
Pyruvate
PKM
ENO3
PGAM2
PGK1
GAPDH
PEP
2PG
3PG
1,3BPG
b)
ECAR (mpH/min)
Male
Female
c)
Hk2
Gp1
Pfkm
Aldoa
Tpi
Gapdh
Pgk1
Pgam2
Eno3
Pkm
Relative amount
Male
Cas+P
Cas+DHT
Cas+Oil
Cas+E2
Female
Ovx+P
Ovx+DHT
Ovx+Oil
Ovx+E2
d)
Pfkfb3 by sequencing
CPM
e)
Pfkfb3 by qRT-PCR
Relative amount
f)
PFKFB3
GAPDH
kDa
50
37
C
M
F
#1
#2
#3
Relative protein expression (PFKFB3/GAPDH)
MS
FS

Figure 11. ***Male-biased glycolytic activity and Pfkfb3 expression.***

a) Illustration of the glycolytic pathway with enzymes shown in yellow boxes and intermediate substances shown in blue boxes is presented. PFKFB3 mediates the reaction that convert F-6-P to F-2,6-BP, the latter of which acts as a strong activator of PFKM. **b)** Male (n=3) and female (n=3) muscle fibers were obtained from type IIB-enriched regions of the quadriceps muscle (Figure 7a). The ECARs of cultured muscle fibers were examined, and the results were corrected by the ratio of the mean protein content in the fibers from the two sexes (male/female = 1.10) (Table 10). **$p<0.01$. **c)** The expressions of glycolytic genes were examined in the 10 experimental mouse groups (Figure 1) by qRT-PCR (n=3 each group). Among paralogous genes, if any, the gene showing the highest expression was assessed. **d)** The expression of *Pfkfb3* was extracted from the transcriptome datasets. **e)** The expression of *Pfkfb3* mRNA was examined by qRT-PCR (n=3 each group). **f)** The amounts of PFKFB3 protein were analyzed by western blotting. Whole proteins obtained from the type IIB-enriched areas of the quadriceps muscles of male (M) and female (F) were used. As a control, HeLa cell lysate was used (C). Western blot images for PFKFB3 (upper left) and GAPDH (lower left) are shown. Three biologically independent samples (#1, #2, and #3) were used. The results were normalized to GAPDH and are presented as means ± SD (right). **$p<0.01$. For **(c)** and **(e)**, the bars (means ± SD) with the same letter are not significantly different from each other ($p<0.01$).

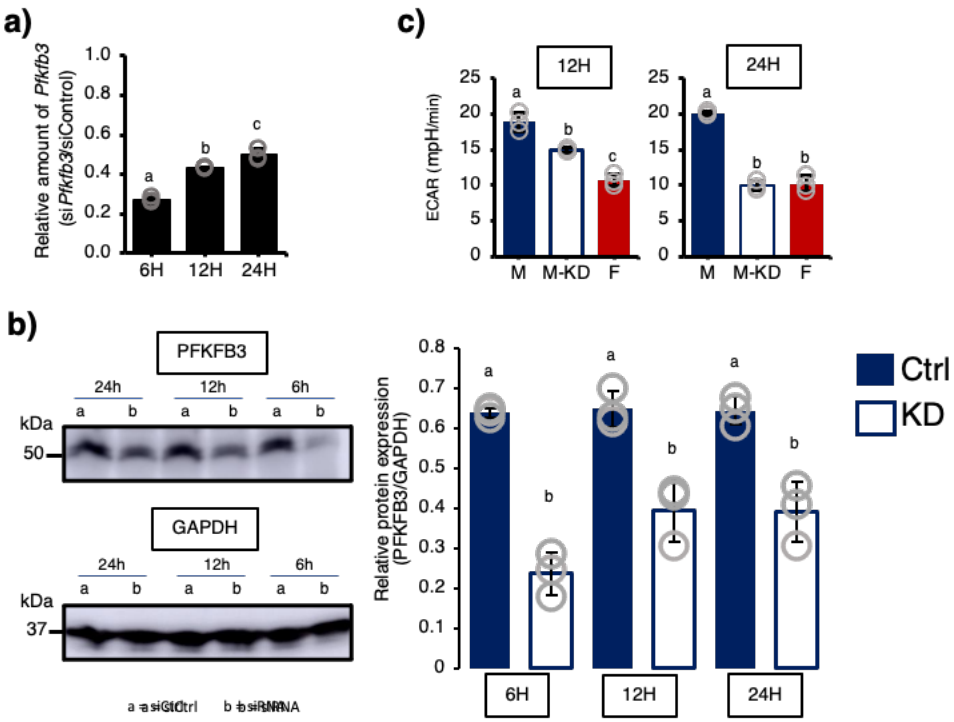

Figure 12. ***Impact of Pfkfb3 knockdown on glycolysis in muscle fibers.***

a) Male quadriceps muscle fibers were transfected with si*Pfkfb3* (n=3) or control siRNA (n=3) for 6, 12, or 24 h. qRT-PCR was used to determine the amount of *Pfkfb3* mRNA. The ratios of the amounts of *Pfkfb3* mRNA in the si*Pfkfb3*- and control siRNA-treated fibers are shown. **b)** The expressions of PFKFB3 and GAPDH were determined by western blotting at 6, 12, and 24 h after the siRNA transfection. The intensities of the PFKFB3 signals were normalized to those of GAPDH, and the relative intensities are presented as means ± SD (n=3 each group). **c)** ECARs were determined in the male-derived fibers treated with control siRNA (M), male-derived fibers treated with si*Pfkfb3* (M-KD), and female-derived fibers treated with control siRNA (F). The fibers were transfected with siRNA for 12 h (left) or 24 h (right). The results were corrected by the ratio of the mean protein content in the fibers from the two sexes. As described in the Methods, the data from three biologically independent samples were analyzed. The bars (means ± SD) with the same letter are not significantly different from each other ($p<0.01$).

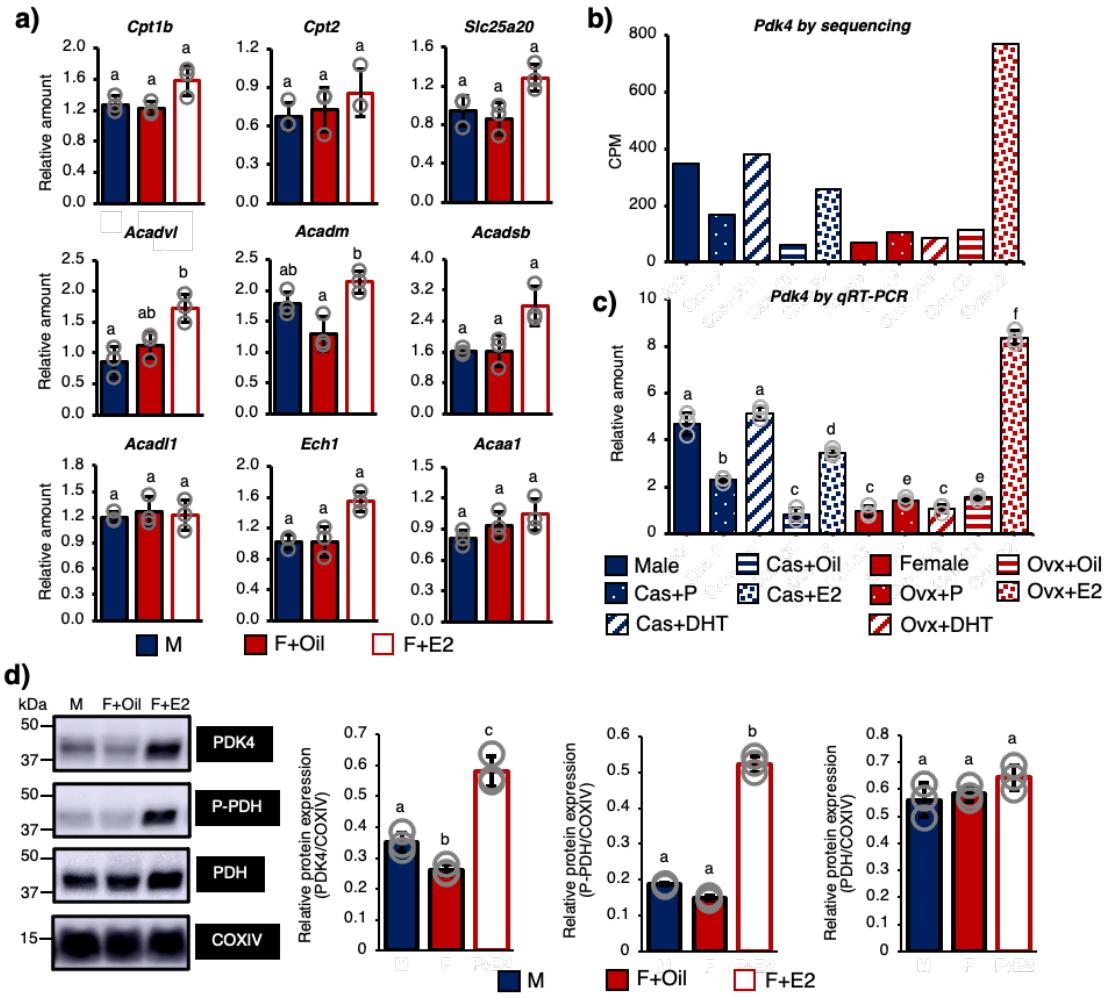

Figure 13. ***Expression of gene related Fatty acid β-oxidation and Pdk4.***

a) Muscle fibers were isolated from male (n=3) (M) and diestrus female treated with oil (n=3) (F+Oil) or E2 for 24 h (n=3) (F+E2). The expression of genes implicated in fatty acid β-oxidation was assessed by qRT-PCR. **b, c)** Quadriceps type IIB fibers were obtained from the 10 experimental mouse groups (Figure 1). The expression profiles of *Pdk4* extracted from the sequence datasets **(b)** and determined by qRT-PCR (n=3 each group) **(c)** are presented. **d)** The muscle fibers used in ***(a)*** were used to examine the protein expressions of PDK4, P-PDH (phosphorylated PDH), and PDH by western blotting. As described in the Methods, the signals were semi-quantified. Signal intensities for PDK4, P-PDH, and PDH were normalized to those of COXIV, and the

relative amounts are presented as means ± SD (n=3 each group). Data were analyzed from three biologically independent samples. The bars (means ± SD) with the same letter are not significantly different from each other ($p<0.01$).

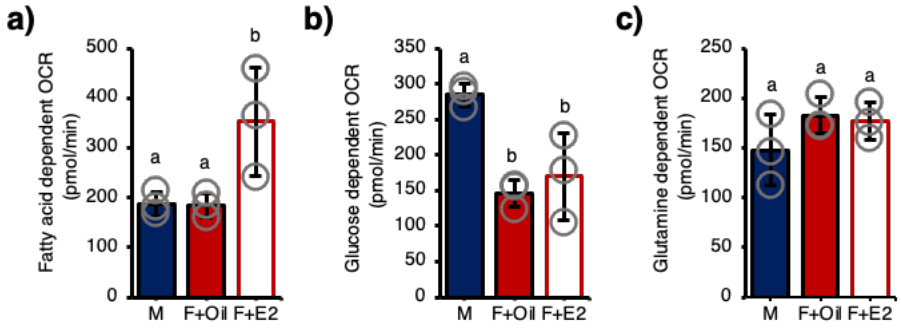

Figure 14. ***Effect of E2 on fatty acid, glucose, and glutamine dependent oxygen consumption in female muscle fibers.***

a) The fatty acid-dependent OCRs result of the fibers are shown (n=3 each group). Glucose **(b)** and glutamine **(c)** dependent OCR were also measured in the E2-treated female muscle fibers. Data from three biologically independent samples were analyzed. The bars (means ± SD) with the same letter are not significantly different from each other ($p<0.01$).

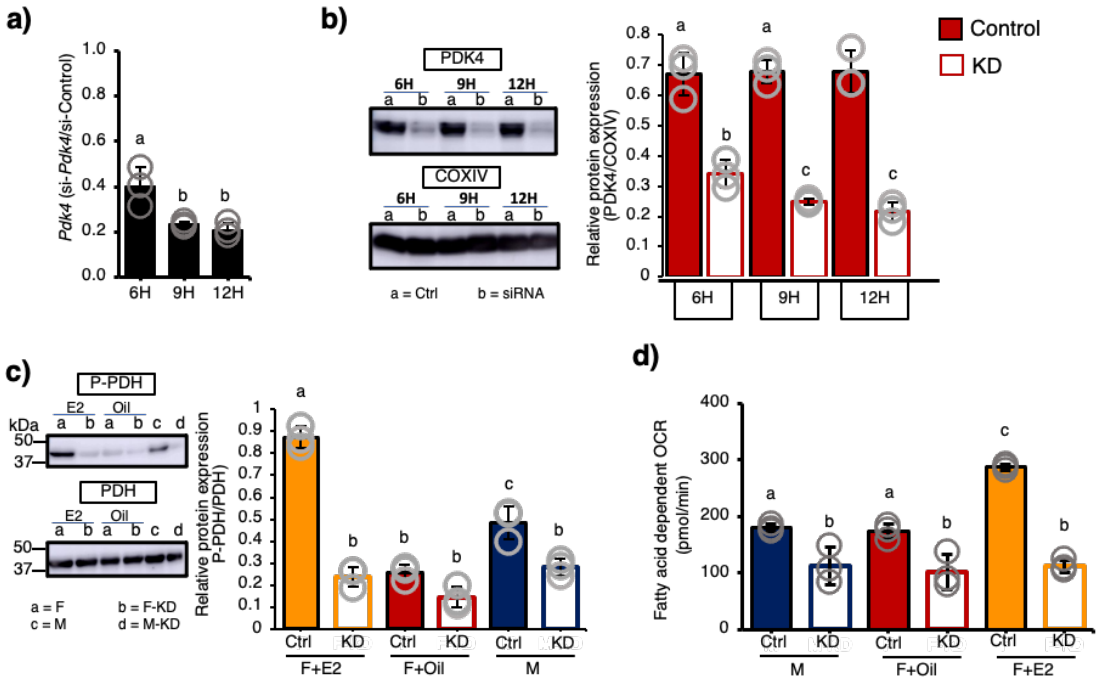

Figure 15. ***Cancellation of fatty acid-dependent OCR by Pdk4 knockdown.***

a) The female muscle fibers were transfected with si*Pdk4* (n=3) or control siRNA (n=3) for 6, 9, or 12 h. The amount of *Pdk4* mRNA was examined by qRT-PCR. Ratios of the amounts of *Pdk4* mRNA between the si*Pdk4*- and control siRNA-treated fibers are indicated. **b)** The effect of knockdown was assessed at the level of PDK4 protein. The intensities of the PDK4 signals were normalized to those of COXIV, and the relative amounts are showed as means ± SD (n=3 each group). **c)** The levels of P-PDH and PDH in the muscle fibers were determined at 9 h after transfection with si*Pdk4* (KD) or control siRNA (Ctrl). The intensity of the P-PDH signals were normalized to those of PDH signals, and the relative amounts are presented as means ± SD (n=3 each group). **d)** The fatty acid-dependent OCR was measured, and the results were corrected by the ratio of the mean protein content in the fibers from the two sexes. Data were analyzed from three biologically independent samples. The bars (means ± SD) with the same letter are not significantly different from each other ($p<0.01$).

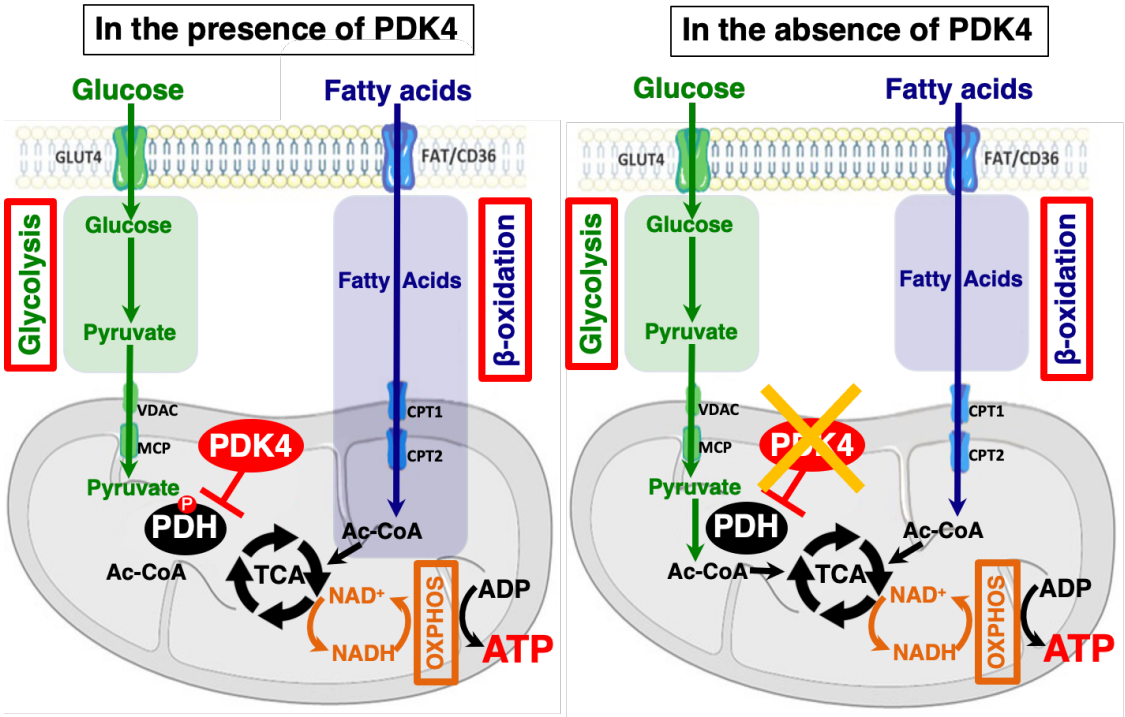

Figure 16. ***The reaction mediated by PDK4.***

In the presence of pdk4, PDH is phosphorylated by PDK4 to become inactive. In this situation, glycolytic product, pyruvate, cannot be utilized for TCA cycle, thus mitochondria utilize fatty acid rather than glucose for ATP production. In the absence of PDK4, PDH (pyruvate dehydrogenase) is not phosphorylated and kept active. PDH converts glycolytic final product pyruvate to Acetyl-CoA, that is utilized for TCA cycle followed by mitochondrial oxidative phosphorylation. Thus, mitochondria can utilize both glucose and fatty acid as the fuel for ATP production.

LIST OF TABLES

Table 1. Evaluation of the cDNA libraries.

Sample	Total reads	Uniquely mapped reads	Reads mapped to multiple loci
Female	18,025,587	15,793,547 (87.6% of total reads)	1,483,012 (9.4% of total reads)
Ovx/Oil	32,300,145	28,298,243 (87.6% of total reads)	2,188,562 (7.7% of total reads)
Ovx/Pellet	21,370,733	18,434,578 (86.3% of total reads)	1,357,928 (7.4% of total reads)
Ovx/DHT	37,483,030	32,849,069 (87.6% of total reads)	3,908,835 (11.9% of total reads)
Ovx/E2	29,106,525	25,037,002 (86.0% of total reads)	1,948,004 (7.8% of total reads)
Male	31,745,787	27,797,207 (87.6% of total reads)	1,400,962 (8.9% of total reads)
Cas/Oil	29,637,802	25,351,649 (85.5% of total reads)	1,634,427 (6.4% of total reads)
Cas/Pellet	22,509,281	18,791,046 (83.5% of total reads)	1,056,558 (5.6% of total reads)
Cas/DHT	45,611,883	39,194,875 (85.9% of total reads)	2,510,912 (6.4% of total reads)
Cas/E2	45,976,100	39,113,030 (85.1% of total reads)	2,893,066 (7.4% of total reads)

Table 2. Nucleotide sequences of the primers used for genotyping and qRT-PCR.

Gene	Forward (5' → 3')	Reverse (5' → 3')
Myh1	CCAAGTGCAGGAAAGTGACC	AGGAAGAGACTGACGAGCTC
Myh2	AAGCGAAGAGTAAGGCTGTC	GTGATTGCTTGCAAAGGAAC
Myh4	CAATCAGGAACCTTCGGAACAC	GTCCTGGCCTCTGAGAGCAT
Myh7	CCAAGGGCCTGAATGAGGAG	GCAAAGGCTCCAGGTCTGAG

Gene	Forward (5' → 3')	Reverse (5' → 3')
Actb	ATCCTGGCCTCACTGTCCACCTTC	AAACGCAGCTCAGTAACAGTCCGC
Aldoa	GCCGCAGCCAGTGAATCTCTCTTC	TTCACAGACAACACCGCACACGAG
Amd2	GACGCATGAATTCTGACTGC	TGGGTCAAGCTCACTCATCA
Eno3	TCCCGTGGTCTCCATTGAG	CCACCCCAGAGAGGAATGAG
Gapdh	TGGTGGACCTCATGGCCTACATGG	TGAGGGAGATGCTCAGTGTTGGGG
Gpi1	AAGGAGGTGATGCAGATGCT	GCCCGATTCTCGGTGTAGT
Hk2	GCACTGGAGAAGAGCTTTTCGA	AGGGACACGCCCTTCATG
Pdk4	GGATTACTGACCGCCTCTTTAGTT	GCATTCCGTGAATTGTCCATC
Pfkfb3	AGAACTTCCACTCTCCCACCCAAA	AGGGTAGTGCCCATTGTTGAAGGA
Pfkm	CGATCTGTGGAGATGCTGAA	AATGGGATCAGATGCAAAGC
Pgam2	TACACCTCCATCAGCAAGGA	GCAATGGTGTCCTTGAGACTT
Pgk1	AAGTCCTTCCTGGGGTGGATGCTC	AGGGTTCCTGGTGCCACATCTCAG
Pkm	TTAGGCCAGCAACGCTTGTAGTGC	AGATGCTGCCGCCCTTCTGTGATA
Smox	GCCAGAGTGGAGAGAATCCG	CTGCCTCTTGAGCACGCCCA
Tpi1	TGAGCCGTTTCCACCGCCCTATTA	GCTCCAACCATGAGTTTCCAGCCC

Gene	Forward (5' → 3')	Reverse (5' → 3')
Acaa1	CCCTGCTACGAGGTGTGTTC	ACATTGCCCACGATGACACT
Acsdl1	TGGCTAACATGTACGCCATCA	ATCTTGGCGATCGCTGAGA
Acadm	AGAGCTCTAGACGAAGCCAC	GAGTTCAACCTTCATCGCCATT
Acadsb	GTTGCTCCTCTGGTTTCCTCTAT	CCTCCATATTGTGCTTCAACTTC
Acadvl	GGAGGACGACACTTTGCAGG	AGCGAGCATACTGGGTATTAGA
Cpt1b	GTCGCTTCTTCAAGGTCTGG	AAGAAAGCAGCACGTTCGAT
Cpt2	GGATAAACAGAATAAGCACACCA	GAAGGAACAAAGCGGATGAG
Ech1	GCTACCGCGATGACAGTTTC	GCTCAGAGATCGAAGGCTGATG
Slc25a20	CATGTGCCTGGTGTTTGTGG	CCCTGTGATGCCCTCTCTCA

Table 3. Expression of genes encoding myosin heavy chain.

Gene	Male	Cas/P	Cas/DHT	Cas/O	Cas/E2	Female	Ovx/P	Ovx/DHT	Ovx/O	Ovx/E2
Myh1	1695.0	2800.4	1428.8	1331.4	1848.9	1737.0	1440.3	1462.9	1697.1	3800.6
Myh2	1380.4	850.4	943.0	997.5	1240.0	1268.1	1008.9	1013.0	1110.9	1004.7
Myh3	132.3	71.0	88.9	87.2	103.7	111.7	92.3	84.2	104.4	90.2
Myh4	66402.5	54104.7	55911.9	58688.9	68386.0	70749.2	59026.2	54514.2	63499.3	53003.8
Myh6	0.9	0.0	0.0	0.1	0.1	0.2	0.0	0.0	0.2	0.0
Myh7	5.0	0.0	0.0	0.1	0.1	0.1	0.3	0.0	0.2	0.1
Myh7b	1.5	1.0	0.6	1.0	1.0	1.5	1.0	1.0	1.2	0.6
Myh8	799.9	516.3	609.4	563.6	742.2	798.2	593.6	620.8	681.2	593.8
Myh9	70.9	95.4	77.7	87.7	60.4	69.7	83.1	103.9	92.3	84.7
Myh10	11.8	13.8	17.9	11.2	20.4	11.4	15.0	14.0	14.4	21.5
Myh11	7.1	10.9	6.0	7.4	5.7	6.3	6.8	10.7	6.5	10.4
Myh13	470.7	315.3	492.1	530.3	571.6	632.3	449.7	472.7	546.1	463.5
Myh14	36.6	32.1	39.9	38.2	42.4	34.8	35.3	47.6	39.1	28.9
Myh15	0.0	0.0	0.0	0.0	0.0	0.0	0.0	0.0	0.0	0.0

Table 4. Lists of male-enriched genes.

Rank	Gene	CPM		FC*
		Male	Female	
1	*Ddx3y*	73.69	0.00	7,370.43
2	*Uty*	22.08	0.00	2,208.98
3	*Eif2s3y*	28.32	0.10	260.68
4	*Kdm5d*	18.37	0.10	169.11
5	*Cyp17a1*	11.70	0.20	56.47
6	*Vaultrc5*	18.12	0.89	20.19
7	*Cish*	42.27	2.52	16.73
8	*Tfcp2l1*	22.47	1.73	12.94
9	*1700001O22Rik*	10.09	0.89	11.25
10	*Npnt*	13.45	1.38	9.67
11	*Amd1*	1,561.74	200.19	7.80
12	*Amd2*	1,561.74	200.19	7.80
13	*Slc30a2*	10.95	1.38	7.88
14	*Atp1b1*	11.91	2.12	5.59
15	*Cdk19*	59.85	11.15	5.36
16	*Igf1*	59.43	11.15	5.33
17	*3000002C10Rik*	11.34	2.17	5.21
18	*Pdk4*	348.89	70.66	4.94
19	*Mafb*	78.72	17.12	4.60
20	*Smox*	468.56	106.53	4.40
21	*Casp12*	11.59	2.57	4.50
22	*Ptpn3*	19.15	4.29	4.45
23	*Chac1*	73.02	17.27	4.23
24	*Timp4*	13.73	3.60	3.80
25	*Npc1*	99.20	26.65	3.72
26	*Tiam1*	29.00	8.49	3.41
27	*Cbr2*	14.16	4.44	3.18
28	*Odc1*	137.33	47.02	2.92
29	*Stab2*	22.26	7.70	2.89
30	*Rcan1*	61.74	21.51	2.87
31	*Pfkfb3*	1,044.88	366.97	2.85
32	*Spon1*	10.70	3.75	2.85
33	*Rcan2*	18.48	6.56	2.81
34	*Jak3*	12.09	4.34	2.78

Rank	Gene	CPM		FC*
		Male	Female	
35	*Lincpint*	27.4	10.0	2.75
36	*Pygo1*	12.3	4.6	2.68
37	*Mettl21c*	83.5	32.3	2.59
38	*Spns2*	75.2	29.2	2.58
39	*Cited2*	71.0	27.6	2.57
40	*Adarb1*	12.4	4.9	2.54
41	*Mb*	30.7	12.2	2.52
42	*Socs2*	23.1	9.4	2.47
43	*Lpl*	47.2	19.5	2.42
44	*Cd24a*	157.7	66.9	2.36
45	*Fabp4*	44.1	18.8	2.36
46	*Serpinb6a*	137.4	59.3	2.32
47	*Sh3d19*	10.5	4.6	2.32
48	*Acsl3*	59.6	26.3	2.28
49	*Fhl1*	19.1	8.4	2.28
50	*Msrb1*	115.3	51.1	2.26
51	*Slc43a3*	11.9	5.3	2.28
52	*Golm1*	20.8	9.5	2.20
53	*Ar*	118.5	54.1	2.19
54	*Cmtm6*	10.4	4.7	2.21
55	*Prkg1*	27.4	12.5	2.19
56	*St3gal5*	23.2	10.7	2.18
57	*Gadl1*	18.4	8.6	2.15
58	*Eda2r*	14.0	6.6	2.16
59	*Unkl*	12.9	6.1	2.13
60	*Slc40a1*	29.4	14.1	2.10
61	*Ece1*	98.6	47.3	2.09
62	*2310061I04Rik*	26.0	12.6	2.07
63	*H60b*	33.6	16.4	2.05
64	*Ttll7*	383.5	188.5	2.04
65	*1810011O10Rik*	10.9	5.4	2.05
66	*Asb15*	36.3	18.1	2.01
67	*Nqo1*	15.48	7.70	2.01
68	*0610009L18Rik*	13.98	6.96	2.01

* fold change (FC) was calculated after adding 0.01 to the original CPM values.

Table 5. Lists of female-enriched genes.

Rank	Gene	CPM		FC*
		Male	Female	
1	*Xist*	346.49	4.57	75.73
2	*Tsix*	45.45	0.86	52.48
3	*Cyp4f39*	22.20	3.42	6.47
4	*Mki67*	10.21	1.78	5.70
5	*Mrc1*	34.05	6.28	5.42
6	*Fgfr4*	10.51	2.35	4.45
7	*Rian*	59.06	13.77	4.29
8	*Igfn1*	91.73	26.86	3.41
9	*Atp9a*	27.19	8.92	3.05
10	*Meg3*	69.62	23.33	2.98
11	*Gramd1b*	36.27	12.56	2.89
12	*Actc1*	4,141.90	1,455.73	2.85
13	*Selenbp1*	10.12	3.57	2.83
14	*Igf2*	71.15	25.54	2.79
15	*Peg3*	75.05	27.89	2.69
16	*Col1a1*	248.54	95.10	2.61
17	*Car3*	3,034.73	1,176.83	2.58
18	*Angpt1*	10.95	4.28	2.56
19	*Fbxl22*	17.22	6.92	2.49
20	*Ces1d*	78.80	32.39	2.43
21	*Itga9*	23.44	9.60	2.44
22	*Stbd1*	84.72	34.85	2.43
23	*Aqp4*	56.50	23.22	2.43
24	*Snx30*	10.51	4.28	2.45
25	*Col3a1*	386.11	159.66	2.42
26	*Mxra8*	23.98	9.95	2.41
27	*Sfxn2*	14.16	5.92	2.39
28	*Lrtm1*	130.07	55.40	2.35
29	*Gm13031*	10.16	4.32	2.35
30	*Padi2*	148.62	64.38	2.31

Rank	Gene	CPM		FC*
		Male	Female	
31	*Hist1h2be*	17.07	7.38	2.31
32	*Loxl1*	11.74	5.07	2.32
33	*Tceal7*	25.56	11.13	2.30
34	*Lmcd1*	31.73	13.88	2.29
35	*6330410L21Rik*	13.03	5.74	2.27
36	*Btg2*	19.79	8.92	2.22
37	*Rhobtb1*	40.02	18.26	2.19
38	*H19*	521.71	239.63	2.18
39	*Kcnc3*	19.15	8.85	2.16
40	*Myc*	10.21	4.71	2.17
41	*Col1a2*	190.96	90.39	2.11
42	*Dpy19l3*	12.39	5.81	2.13
43	*Lgmn*	23.59	11.13	2.12
44	*Foxo6*	20.18	9.52	2.12
45	*Col18a1*	11.60	5.46	2.12
46	*Kazald1*	10.16	4.78	2.12
47	*Pnpla3*	18.01	8.60	2.09
48	*Mustn1*	14.75	7.06	2.09
49	*Itm2a*	181.34	87.46	2.07
50	*B230312C02Rik*	106.19	51.26	2.07
51	*C130080G10Rik*	20.92	10.06	2.08
52	*St6galnac4*	20.92	10.06	2.08
53	*Thbd*	21.12	10.27	2.05
54	*Gm5105*	72.19	35.35	2.04
55	*Obsl1*	204.28	100.23	2.04
56	*Tbc1d1*	67.95	33.42	2.03
57	*Fam20c*	39.47	19.44	2.03
58	*Adamts2*	24.08	11.88	2.03
59	*Glt28d2*	18.70	9.24	2.02
60	*Entpd4*	446.86	223.22	2.00

* fold change (FC) was calculated after adding 0.01 to the original CPM values.

Table 6. List of GO terms related to male-enriched (upper) and female-enriched (lower) with $p < 10^3$.

Male-enriched genes

GO terms	p-value
Polyamine biosynthetic process	4.8E-04
Cholesterol homeostasis	1.2E-03
Positive regulation of activated T cell proliferation	2.9E-03
Regulation of gene expression	3.5E-03
Response to hypoxia	3.8E-03
S-Adenosylmethioninamine biosynthetic process	6.6E-03
Response to oxidative stress	9.8E-03

Female-enriched genes

GO terms	p-value
Collagen fibril organization	1.8E-04
Wound healing	2.4E-03
Skeletal system development	3.4E-03
Positive regulation of catalytic activity	5.4E-03
Regulation of phosphorus metabolic process	8.4E-03

Table 7. Female-biased collagen gene expression.

Gene	Male	Cas+P	Cas+DHT	Cas+O	Cas+E2	Female	Ovx+P	Ovx+DHT	Ovx+O	Ovx+E2
Col1a1	95.1	193.7	127.3	184.9	244.1	248.5	258.3	253.9	222.6	267.1
Col1a2	90.4	158.4	175.1	156.5	182.0	191.0	230.3	281.8	187.5	231.8
Col3a1	159.7	392.3	395.0	337.6	227.0	386.1	482.5	733.4	413.1	307.0
Col4a1	158.2	303.5	323.7	239.4	176.2	197.6	273.5	364.8	235.8	268.0
Col4a2	110.0	205.3	187.6	156.2	112.0	118.8	190.3	224.1	159.5	180.1
Col5a1	44.1	69.1	73.5	57.8	49.6	65.5	71.9	120.3	65.4	65.6
Col5a2	19.7	38.8	39.5	29.0	25.4	32.0	38.4	61.6	34.9	36.5
Col5a3	43.8	61.3	81.1	49.3	45.7	71.2	85.3	121.1	79.4	88.6
Col6a1	34.4	73.4	67.5	46.7	45.2	39.0	88.9	90.6	69.5	77.2
Col6a2	30.8	74.9	71.0	60.0	52.1	47.2	89.4	101.0	71.5	87.3
Col6a3	77.1	161.5	131.4	120.3	95.6	107.9	190.4	183.0	140.3	169.2
Col6a6	14.1	20.6	24.4	18.3	4.0	13.3	26.1	30.4	22.9	9.9
Col7a1	21.0	25.3	55.4	22.4	18.1	18.0	21.2	49.1	19.5	13.0
Col15a1	39.3	117.7	86.1	77.8	33.0	53.2	100.0	72.1	86.4	81.1
Col22a1	13.8	51.7	27.7	21.0	56.3	17.7	30.6	17.7	17.8	41.6

Table 8. CPM value of *Pfkfb3* and glycolytic genes.

Gene	TPM									
	Male	Cas/O	Cas/P	Cas/ DHT	Cas/ E2	Female	Ovx/O	Ovx/P	Ovx/DHT	Ovx/ E2
Pfkfb3	1044.9	307.0	365.5	558.2	156.5	366.9	509.2	464.5	301.9	669.7
Pdk4	348.9	70.7	60.7	114.2	168.9	104.6	381.8	85.5	257.4	769.7
Gck	7.5	2.1	0.4	0.2	0.5	0.1	3.3	11.5	1.5	3.3
Slc2a3	3.8	1.5	0.2	1.4	0.1	0.7	11.0	13.5	0.8	1.8
Hk2	260.0	303.9	316.2	514.2	329.1	301.4	268.3	253.9	370.3	281.2
Gpi1	890.9	880.8	725.6	796.1	852.6	790.6	820.6	747.9	804.5	733.0
Pfkm	3232.1	2984.9	3050.1	3230.8	3248.1	2637.5	2932.1	2819.8	3184.6	3231.4
Aldoa	13505.3	13763.1	10850.6	13413.6	15924.7	13538.3	12586.0	12426.9	13589.8	14484.2
Tpi1	1680.3	1752.6	1296.6	1619.1	2034.2	1623.5	1583.1	1521.9	1642.9	1649.9
Gapdh	3627.3	2850.9	2211.1	3130.1	3625.7	3180.4	2658.8	2690.9	3112.3	3536.2
Pgk1	625.2	736.9	532.7	679.6	911.1	738.3	652.3	679.3	620.6	753.4
Pgam2	1295.1	1092.7	908.5	1089.4	1314.4	1151.9	1049.9	985.2	1023.5	964.4
Eno3	4145.6	5181.8	3986.2	4765.6	5867.4	5286.9	4744.2	4471.5	4649.6	4969.7
Pkm	3224.2	3158.3	2527.6	3095.3	3549.7	3278.9	2994.3	2865.3	3289.5	2962.8

Table 9. CPM value of β-oxidation genes in the 10 experimental groups.

Gene	Male	Cas+P	Cas+DHT	Cas+O	Cas+E2	Female	Ovx+P	Ovx+DHT	Ovx+O	Ovx+E2
Acsf3	13.63	11.95	11.69	15.92	12.54	13.03	11.73	13.77	12.42	13.69
Acsl1	158.20	120.46	148.18	103.13	147.88	137.67	122.59	120.09	127.54	221.43
Acsl3	59.53	33.31	58.20	22.86	26.68	26.15	19.80	39.08	17.47	15.89
Acsl4	37.49	36.56	41.58	40.47	33.98	41.10	33.86	33.00	37.04	37.93
Acsl6	44.98	44.53	47.20	45.89	42.84	41.05	41.74	45.96	42.34	34.82
Acss1	8.13	20.55	15.68	15.42	12.15	10.21	12.25	7.44	10.56	14.25
Acss2	15.41	19.58	17.72	16.47	16.96	15.25	11.80	13.40	17.07	24.63
Cpt1b	194.19	187.61	203.58	176.81	196.93	161.75	175.75	188.82	172.95	217.06
Cpt2	29.11	30.69	35.08	30.25	28.35	26.65	23.87	29.29	27.93	32.90
Slc25a20	20.65	22.62	20.57	14.03	22.15	15.35	16.25	16.56	18.93	30.81
Acad11	50.65	62.43	50.48	55.25	63.60	58.42	50.57	37.52	56.81	52.41
Acad12	14.59	21.78	17.32	17.80	19.23	14.31	15.91	14.53	18.37	13.05
Acad8	17.12	24.19	23.99	19.60	23.09	22.01	21.19	22.47	16.40	24.52
Acad9	24.15	21.95	25.50	25.21	24.79	22.75	22.55	25.14	23.80	27.08
Acadl	54.43	66.24	61.18	47.63	73.54	46.73	39.97	48.30	56.40	105.59
Acadm	104.55	95.78	115.06	83.48	110.30	78.31	75.75	84.38	86.88	123.38
Acads	27.64	36.18	35.24	36.23	42.82	32.71	30.09	38.49	34.46	37.24
Acadsb	77.73	79.91	75.07	85.14	89.96	82.31	88.54	59.26	83.95	94.77
Acadvl	100.48	116.30	119.52	105.62	134.64	100.22	104.79	106.64	110.91	160.56
Ech1	47.30	49.18	58.29	52.84	62.89	49.29	54.75	48.58	53.49	73.22
Echdc1	24.11	15.97	20.07	18.74	18.69	19.24	17.53	15.25	15.20	19.26
Echs1	31.50	60.47	38.27	50.07	54.04	34.44	41.93	29.17	41.22	52.55
Hadh	61.92	44.57	60.38	51.95	63.36	47.52	46.68	52.78	53.29	58.78
Hadha	165.01	148.77	153.96	145.95	165.29	139.94	136.99	151.93	146.50	185.27
Hadhb	135.55	140.63	147.37	133.60	143.49	126.47	118.78	125.38	123.08	149.82
Acaa1a	21.90	25.38	28.59	28.15	34.11	30.20	27.87	25.95	28.31	26.25
Acaa2	31.85	46.63	37.23	33.38	49.47	31.38	27.60	26.85	34.39	57.92

Table 10. Amounts of proteins of male and female type IIB fibers of quadriceps.

Sample	µg protein/fibers		Average	M/F
	Left	Right		
M1	18.64	18.53	18.59	1.10
M2	19.54	19.81	19.68	
M3	19.34	19.23	19.29	
F1	16.71	17.30	17.01	
F2	17.53	17.78	17.66	
F3	17.48	17.39	17.44	